

# Fully distributed and resilient source seeking for robot swarms

Jesús Bautista, Antonio Acuaviva, José Hinojosa, Weijia Yao, Juan Jiménez, Héctor García de Marina

**Abstract**—We propose a self-contained, resilient and fully distributed solution for locating the maximum of an unknown 3D scalar field using a swarm of robots that travel at constant speeds. Unlike conventional reactive methods relying on gradient information, our methodology enables the swarm to determine an ascending direction so that it approaches the source with an arbitrary precision. Our source-seeking solution consists of three algorithms. The first two algorithms run sequentially and distributively at a *high* frequency providing barycentric coordinates and the ascending direction respectively to the individual robots. The third algorithm is the individual control law for a robot to track the estimated ascending direction. We show that the two algorithms with higher frequency have an exponential convergence to their eventual values since they are based on the standard consensus protocol for first-order dynamical systems; their high frequency depends on how fast the robots travel through the scalar field. The robots are not constrained to any particular geometric formation, and we study both discrete and continuous distributions of robots within *swarm shapes*. The *shape analysis* reveals the resiliency of our approach as expected in robot swarms, i.e., by amassing robots we ensure the source-seeking functionality in the event of missing or misplaced individuals or even if the robot network splits in two or more disconnected subnetworks. In addition, we also enhance the robustness of the algorithm by presenting conditions for *optimal* swarm shapes, in the sense that the ascending directions can be closely parallel to the field’s gradient. We exploit such an analysis so that the swarm can adapt to unknown environments by morphing its shape and maneuvering while still following an ascending direction. We analyze our solution with robots as kinematic points in  $n$ -dimensional Euclidean spaces and extend the analysis to unicycle-like robots with constant speeds in 3D. Finally, we end with numerical validations involving hundreds of robots.

## I. INTRODUCTION

### A. Motivation and aim

The ability to detect and surround sources of chemicals, pollution, and radio signals effectively with robot swarms will enable persistent missions in vast areas for environmental monitoring, search & rescue, and precision agriculture operations [1]–[5]. In particular, seeking the source of a scalar field can be regarded as one fundamental task in swarm

robotics [6], [7] where the resiliency of the robot swarm is expected, i.e., the swarm preserves its functionality against unexpected adverse conditions, unknown, possibly unmodeled, disturbances and the malfunctioning of robot individuals. However, formal guarantees on the performance of a solution while remaining feasible in practice, e.g., by fitting into realistic robot dynamics, communications, and scalability, are one of the great challenges in swarm robotics [6]–[8]. In this regard, we present and rigorously analyze a distributed source-seeking algorithm for robot swarms, including non-holonomic ones in 3D, where the source is reached even if individuals go missing during the mission.

### B. Overview of our source-seeking algorithm

Before starting the literature review, we want to outline the key features of our solution to facilitate a fair comparison with existing algorithms in the next subsection. Now, we will discuss what makes our algorithm appealing for different scenarios and robot dynamics in source-seeking missions.

Our algorithm guarantees with sufficient conditions an ascending direction rather than the gradient in order to guide the centroid of the robot swarm to the source of a scalar field, i.e., all the individual robots estimate distributively and track a common ascending direction. Indeed, considering an ascending direction offers more flexibility to the robot swarm since there are multiple ones instead of the single gradient direction. The algorithm does not require a specific formation or shape for the robot swarm; in fact, we will show how the computed ascending direction reacts to the relation of the swarm shape and the scalar field. This fact will be exploited to maneuver the robot swarm by morphing its shape while getting closer to the source simultaneously. The non-requirement of a specific shape allows for missing robots without compromising the performance of the algorithm, as the resultant formation also ensues an ascending direction.

The mathematical expression on how to calculate the ascending direction allows us to jump from discrete robots to a continuous distribution of them. Indeed, the analysis of the swarm shape and the density of the robot distribution within allows us to guarantee *optimal shapes* so that the calculated ascending direction is parallel to the actual gradient. Of course, the algorithm is implemented in discrete robots eventually; notwithstanding, the *continuous* results are fairly achieved with a density of robots sufficiently high, i.e., a swarm. The ascending direction can be calculated distributively based on a consensus algorithm. Finally, sharing the same network, we present a distributed algorithm to estimate the swarm centroid since robots need it for the ascending direction estimation.

Bautista and Acuaviva contributed equally as first authors in this publication. Jesús Bautista, Josú Hinojosa, and H. García de Marina are with the Department of Computer Engineering, Automation, and Robotics, and the Research Centre for Information and Communication Technologies (CITIC-UGR), University of Granada, Granada, Spain. A. Acuaviva is with the Department of , University of Lancaster, United Kingdom. J. Jimenez is with the Department of Computer Architecture and Automation, Universidad Complutense de Madrid, Spain. Weijia Yao is with the School of Robotics, Hunan University; he is also with ENTEG, University of Groningen, the Netherlands. Corresponding author e-mail: hgdemarina@ugr.es. The work of H.G. de Marina is supported by the grant Ramon y Cajal RYC2020-030090-I from the Spanish Ministry of Science, and the ERC Starting Grant iSwarm 101076091.

The presented solution is fully compatible with single integrator robots, and with the restrictive but more realistic unicycle robots with constant speeds. Indeed, inspired by the analysis on how unicycles can track guiding vector fields [9], [10], we show how a team of 3D unicycles with constant speeds can track a vector field consisting of ascending directions by employing geometrical controllers [11], and how the centroid of the team gets arbitrarily close to the source eventually. The nature of our swarm algorithm is purely reactive to the field, and it does not need scouting or gathering prior information about the scalar field, and it does not consider a bounded map either. In that regards, our algorithm is mainly suited to work in scalar fields with only one source point and whose gradient and Hessian are bounded.

### C. Existing algorithms: comparisons and trade-offs

This subsection aims to review the pros and cons of source-seeking algorithms fairly popular in the literature. We keep in mind that robot systems are tailored to specific missions and requirements, e.g., robot dynamics, traveled distance, or even prior knowledge of the scenario, i.e., to the best of our knowledge, there is no better algorithm than other in every single metric regarding source-seeking missions.

The popular field-climbing methods focus on estimating the gradient, and possibly the Hessian too, of an unknown scalar field. In [12], [13], the gradient estimation occurs in a distributed manner, where each robot calculates the different gradients at their positions. Since each local gradient is different, a common direction for the team is achieved through a distance-based formation controller that maintains the cohesion of the robot swarm. It is worth noting that this method fails when a subset of neighboring robots adopts a *degenerate* shape, like a line in a 2D plane. In addition, the formation shape and following the gradient in [12], [13] are not fully compatible tasks and they disturb each other, affecting the mission performance. Alternatively, in [14], [15], the gradient and Hessian are estimated at the centroid of a circular formation consisting of unicycles. However, this methodology is relatively rigid due to its mandatory circular shape. Such a formation of unicycles is also present in [16], although robots are not required to measure relative positions but rather relative headings. In contrast to our algorithm, which calculates an ascending direction instead of the gradient, our robot team enjoys greater flexibility concerning formation shapes while still offering formal guarantees for reaching the source. Finally, related to following the gradient but assuming its field is known, we can find the pioneering work [1].

Extremum seeking is another technique employed extensively as discussed in [17]–[19]. In these studies, robots, which could potentially be just one, with nonholonomic dynamics execute periodic movements to facilitate a gradient estimation. However, when multiple robots are involved, there is a necessity for the exchange of estimated parameters. Furthermore, the eventual trajectories of the robots are often characterized by long and cumbersome paths with abrupt turns.

In contrast, our algorithm generates smoother trajectories, albeit requiring more than two robots in 2D.

All the algorithms above require communication among robots sharing the strength of the scalar field. Nonetheless, the authors in [20] offer an elegant solution involving the principal component analysis of the field that requires no sharing of the field strength. However, the centroid of the swarm is still necessary and communication might be in order to estimate it. It is worth noting that in [20] the initial positions of the robots determine the (time-varying) formation during the mission, and it is not under control. In comparison, although our algorithm requires the communication among the robots due to the usage of a consensus algorithm, it is compatible with formation control laws so that it makes the trajectory of the robots more predictable.

Another family of source-seeking algorithms is information-based, which differs from the previously discussed algorithms, including our proposed one, as they are not purely reactive to the field. Information-based strategies can handle multiple sources but at the cost of requiring prior knowledge of the field, or at least they necessitate additional stages before seeking in order to estimate or scout the scalar field. However, the performance of these algorithms is more often supported by compelling experimental evidence rather than analytical proofs [21]–[23]. In connection with information-based algorithms, we conclude this review by briefly discussing a related problem, namely, the mobile-sensing coverage problem [24], [25]. Algorithms addressing this problem are particularly effective at handling multiple sources simultaneously with a robot swarm. They primarily rely on partitioning the area using Voronoi cells. However, this performance comes at a higher cost compared to typical source-seeking solutions: individual robots require dense or continuous information about the scalar field within their corresponding Voronoi cell, and the area to be covered must be predetermined.

### D. Extensions from our previous conference paper

Regarding the evolution of this journal paper concerning our previous conference work [26], we present and address the following new points:

- We show a deployment based on degenerated shapes, i.e., perpendicular lines of robots, to estimate the gradient of the scalar field. We show that the key idea to estimate an ascending direction lies on the variance of the robot distribution.
- We show how the ascending direction can be computed distributively by just requiring a connected network.
- In order to provide a self-contained solution, we present a distributed algorithm rigorously to estimate the centroid of the robot swarm. It can share the same connected network from the previous point.
- In order to cover more realistic robots, we analyze the compatibility of our methodology rigorously with robot teams consisting of 3D unicycles travelling with constant speeds. We exploit geometric controllers for the tracking of vector fields by 3D robots.

- We provide extensive numerical simulations of the previous points validating the theoretical results.

### E. Organization

The article is organized as follows. In Section II, we introduce notations, the considered robot dynamics and assumptions on the considered scalar field to formally state our source-seeking problem. We continue in Section III on how to calculate an ascending direction and how a *swarm* can be represented as a continuum distribution of robots. Also, in the same section, we analyze the sensitivity of the ascending direction concerning the swarm and the observability of the gradient. We present the architecture of the source-seeking solution in Section IV. We first show how the ascending direction can be calculated distributively, then we show the compatibility of our solution with a standard displacement-based formation control algorithm, and finally, we provide a distributed centroid estimator in order to have a self-contained paper. In Sections V and VI, we analyze the tracking of the ascending direction by robots modeled as single integrators and 3D unicycles, respectively, travelling with a constant speed. We validate our theoretical findings in Section VII involving hundreds of robots. Finally, we end this article in Section VIII with some conclusions and future work.

## II. PRELIMINARIES AND PROBLEM FORMULATION

### A. Generic notation

Given a matrix  $A \in \mathbb{R}^{p \times q}$ , we define the operator  $\bar{A} := A \otimes I_m \in \mathbb{R}^{pm \times qm}$ , where  $\otimes$  denotes the Kronecker product and  $I_m$  is the identity matrix with dimension  $m \in \{2, 3\}$ . We also denote by  $\mathbf{1}_p \in \mathbb{R}^p$  the all-one column vector, by  $\|\cdot\|$  the standard 2-norm operator, and by  $A^\top$  the transpose of the vector/matrix  $A$ .

### B. Graph Theory

Since our proposed source-seeking solution consists of distributed algorithms, we need to introduce some notions from Graph Theory [27] in order to define the relations between the robots precisely. Consider a group of  $N$  robots, then a *graph*  $\mathcal{G} = (\mathcal{V}, \mathcal{E})$  consists of two non-empty sets: the node set  $\mathcal{V} = \{1, \dots, N\}$  where each node  $i$  corresponds to the robot  $i$ , and the ordered edge set  $\mathcal{E} \subseteq (\mathcal{V} \times \mathcal{V})$  defining the communications or sensing between pairs of different robots. For an arbitrary edge  $\mathcal{E}_k = (\mathcal{E}_k^{\text{head}}, \mathcal{E}_k^{\text{tail}})$ , we call its first and second element the *tail* and the *head* respectively. The set  $\mathcal{N}_i$  containing the neighbors of the node  $i$  is defined by  $\mathcal{N}_i := \{j \in \mathcal{V} : (i, j) \in \mathcal{E}\}$ .

We only deal with the special case of *undirected* graphs throughout the article, i.e., all the edges  $\mathcal{E}_k$  are considered *bidirectional*, i.e., if  $(i, j) \in \mathcal{E}$  then it implies that  $(j, i) \in \mathcal{E}$ . For an undirected graph, we choose only one of these two arbitrary directions between nodes  $i$  and  $j$ , so that we can construct the *incidence matrix*  $B \in \mathbb{R}^{|\mathcal{V}| \times |\mathcal{E}|}$  of  $\mathcal{G}$

$$b_{ik} := \begin{cases} +1 & \text{if } i = \mathcal{E}_k^{\text{tail}} \\ -1 & \text{if } i = \mathcal{E}_k^{\text{head}} \\ 0 & \text{otherwise.} \end{cases} \quad (1)$$

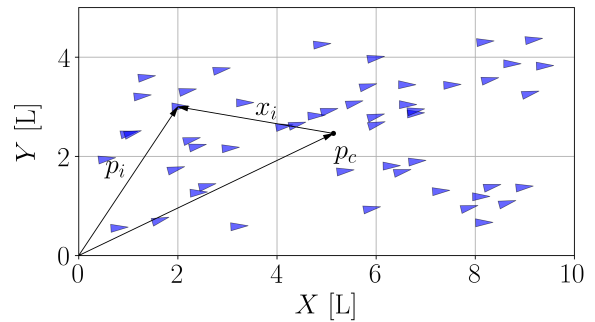


Fig. 1. Deployment  $x$  of a robot swarm with centroid at  $p_c$ .

For an undirected graph, the *Laplacian matrix*  $L \in \mathbb{R}^{|\mathcal{V}| \times |\mathcal{V}|}$  [27, Chapter 6] can be calculated as follows

$$L = BB^\top. \quad (2)$$

If the graph  $\mathcal{G}$  is *connected* [27, Chapter 3], then the Laplacian matrix  $L$  has a single eigenvalue equal to zero, whose associated eigenvector is  $\mathbf{1}_N$  since  $B^\top \mathbf{1}_N = 0$ ; thus,  $L$  is positive semidefinite.

### C. Robot dynamics

In the team of  $N$  robots, the position of the  $i \in \{1, \dots, N\}$  robot in the Euclidean space is represented by  $p_i \in \mathbb{R}^m$ . We define  $p \in \mathbb{R}^{mN}$  as the stacked vector of the positions of all robots in the team, and the centroid of the team as  $p_c := \frac{1}{N} \sum_{i=1}^N p_i$ ; therefore, we can write  $p_i = p_c + x_i$ , where  $x_i \in \mathbb{R}^m$  for all  $i \in \{1, \dots, N\}$ , the barycentric coordinates, describes how the robots are spread around their centroid as it is shown in Figure 1.

**Definition 1.** The *deployment* of a robot team is defined as the stacked vector  $x := [x_1^\top, \dots, x_N^\top]^\top \in \mathbb{R}^{mN}$ . We say that a deployment is not *degenerated* if all  $x_i$ 's span  $\mathbb{R}^m$ .

Therefore, a necessary condition for a deployment not being degenerated is that  $N > m$ .

We will focus on two kinds of robot dynamics for our source-seeking algorithm in 2D and 3D: the single integrator and the unicycle with constant speed. In the former case, the robot can directly track the guiding velocity. In contrast, the robot in the latter case can only actuate on its angular velocities to align its heading with the ascending direction.

The single integrator for the robot  $i$  is modeled by

$$\dot{p}_i = u_i, \quad (3)$$

where  $u_i \in \mathbb{R}^m$  is the guiding velocity as control action. Indeed, the guiding velocity will be the unit vector of the ascending direction.

We will analyze the dynamics of the 3D unicycle using notation and controllers from geometric control [28]. Following the spirit in [29] for roboticists and to mostly focus on our source-seeking algorithm, we have derived from scratch well-known concepts in a detailed way in [30] on differential geometry and geometric controllers to assist with the presented work. In particular, we will borrow

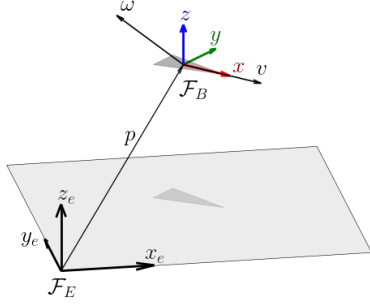


Fig. 2. This figure illustrates a 3D unicycle robot moving at a linear velocity  $v$  and rotating at an angular velocity  $\omega$ . These velocities are observed from the inertial frame  $\mathcal{F}_E$  but represented in the non-inertial frame  $\mathcal{F}_B$ , which is fixed at the body of the robot.  $\{x_e, y_e, z_e\}$  and  $\{x, y, z\}$  are the vector bases of  $\mathcal{F}_E$  and  $\mathcal{F}_B$ , respectively.

such concepts to design the body angular velocities, i.e., the actuators, of the unicycles such that we align the swarm with a vector field or ascending directions. Let us technically start with the following dynamics

$$\begin{cases} \dot{p}_i(t) = R_i(t)v \\ \dot{R}_i(t) = R_i(t)\Omega_i \end{cases}, \quad (4)$$

where  $v = [1 \ 0 \ 0]^\top$ , i.e., the robot is moving with constant speed alongside its  $X$ -axis as it is shown in Figure 2, and the matrix  $R_i \in \text{SO}(3)$  represents the attitude of the robot between  $\mathcal{F}_E$  and  $\mathcal{F}_B$  as in Figure 2. The skew-symmetric matrix  $\Omega_i = \begin{bmatrix} 0 & -\omega_z & \omega_y \\ \omega_z & 0 & -\omega_x \\ -\omega_y & \omega_x & 0 \end{bmatrix} \in \mathfrak{so}(3)$  is built from  $\omega_i = [\omega_x \ \omega_y \ \omega_z]^\top$  which are the robot's angular velocities as the actuators. The construction of  $\Omega$  from  $\omega$  is the standard linear map  $\text{hat} \wedge : \mathbb{R}^3 \rightarrow \mathfrak{so}(3)$ , i.e., the transformation of a given vector  $x \in \mathbb{R}^3$  to a skew-symmetric matrix  $x^\wedge \in \mathbb{R}^{3 \times 3}$ . For the *recovery* of  $\omega$  from a given  $\Omega$  we define the linear map  $\text{vee} \vee : \mathfrak{so}(3) \rightarrow \mathbb{R}^3$  as the opposite of the hat map, i.e.,  $\omega = \Omega^\vee$ .

#### D. The scalar field

The strength of a signal throughout the space can be described by a scalar field.

**Definition 2.** A *signal* is a scalar field  $\sigma : \mathbb{R}^m \rightarrow \mathbb{R}^+$  which is  $C^2$  and all its partial derivatives up to second order are bounded uniformly. Also,  $\sigma$  has only one maximum at  $p_\sigma \in \mathbb{R}^m$ , i.e., the source of the signal, and its gradient at  $a \in \mathbb{R}^m$  satisfies  $\nabla\sigma(a) \neq 0 \iff a \neq p_\sigma$  and  $\lim_{|a| \rightarrow \infty} \sigma(a) = 0$ .

Our definition of signal fits plenty of models in our physical world, especially the signals that fade from the source according to the power law  $x^{-\alpha}$  with  $2 \leq \alpha \leq 3$  where the model starts after considering a minimum fixed distance  $x_{\min}$  from the origin [31], and Gaussian distributions. These signals strengths can represent the modulus of the electromagnetic field, the concentration of a contaminant, or heat radiation. In particular, quadratic scalar fields are relevant in the physical world if we consider the inverse of the power law  $x^{-2}$  or the logarithm of a Gaussian distribution.

In this paper, the gradient is defined as a column vector, i.e.,  $\nabla\sigma(\cdot) \in \mathbb{R}^m$ , and according to our definition of a signal:

$$\|\nabla\sigma(a)\| \leq K \quad \text{and} \quad \|H_\sigma(a)\| \leq 2M, \quad \forall a \in \mathbb{R}^m, \quad (5)$$

where  $K, M \in \mathbb{R}^+$ , and  $H_\sigma$  is the Hessian of the scalar field  $\sigma$ , i.e.,  $H_\sigma(a) \in \mathbb{R}^{m \times m}$ ; thus, from the Taylor series of  $\sigma$  at  $a \in \mathbb{R}^m$  [32, Theorem 5.15], it follows that

$$|\sigma(a) - \sigma(b) - \nabla\sigma(a)^T(a-b)| \leq M\|a-b\|^2, \quad \forall b \in \mathbb{R}^m. \quad (6)$$

Now, we are ready to define the source-seeking problem.

**Problem 1** (source seeking). Given an unknown signal  $\sigma$  and a constant  $\epsilon \in \mathbb{R}^+$ , find control actions for (3) and (4) such that  $\|p_c(t) - p_\sigma\| < \epsilon, \forall t \geq T$  for some finite time  $T \in \mathbb{R}^+$ .

### III. THE ASCENDING DIRECTION

#### A. Discrete robots

The authors in [14] show that for a circular formation of  $N \geq 3$  robots that are equally *angle-spaced*, the expression

$$\hat{\nabla}\sigma(p_c) := \frac{2}{ND^2} \sum_{i=1}^N \sigma(p_i)(p_i - p_c), \quad (7)$$

is an estimation of the gradient at the center  $p_c$  of the circumference with radius  $D$ . However, it is unclear how well (7) approximates the gradient for any generic deployment other than the circle; for example, what is its sensitivity to misplaced robots or if an individual is missing? In fact, without apparently major changes, the expression (7) can be extended significantly by admitting any generic deployment  $x$ , i.e., we will prove that the vector

$$\begin{aligned} L_\sigma(p_c, x) &:= \frac{1}{ND^2} \sum_{i=1}^N \sigma(p_i)(p_i - p_c) \\ &= \frac{1}{ND^2} \sum_{i=1}^N \sigma(p_c + x_i)x_i, \end{aligned} \quad (8)$$

is an ascending direction at  $p_c$  for some mild conditions, where now  $D = \max_{1 \leq i \leq N} \|x_i\|$ . We remark that (8), unlike (7), is a function of a generic deployment  $x$ , and that the ascending direction is not necessarily parallel to the gradient. Such a *non-property* will be an advantage to maneuver the swarm by just morphing  $x$ , or to guarantee an ascending direction in the case of misplaced or missing robots.

Let us approximate  $\sigma(p_c + x_i)$  in (8) to a two-term Taylor series for *small*  $\|x_i\|$ , i.e.,  $\sigma(p_c + x_i) \approx \sigma(p_c) + \nabla\sigma(p_c)^T x_i$ , so that  $L_\sigma(p_c, x) \approx L_\sigma^0(p_c, x) + L_\sigma^1(p_c, x)$ , where  $L_\sigma^0(p_c, x) = \frac{1}{ND^2} \sum_{i=1}^N \sigma(p_c)x_i = 0$  since  $\sum_{i=1}^N x_i = 0$ , and

$$L_\sigma^1(p_c, x) = \frac{1}{ND^2} \sum_{i=1}^N (\nabla\sigma(p_c)^T x_i) x_i. \quad (9)$$

Although the primary property of  $L_\sigma^1$  lies in its direction, the factor  $\frac{1}{ND^2}$  ensures that  $L_\sigma^1$  shares the same physical units as the gradient. The direction of the vector  $L_\sigma^1$  is interesting because, if  $x$  is non-degenerate, then it is an *always-ascending* direction, in the sense that no more conditions are necessary, towards the source  $p_\sigma$  at the centroid  $p_c$ .

**Lemma 1.**  $L_\sigma^1(p_c, x)$  is an always-ascending direction at  $p_c$  towards the maximum  $p_\sigma$  of the scalar field  $\sigma$  if the deployment  $x$  is non-degenerate and  $p_c \neq p_\sigma$ .

*Proof.*  $L_\sigma^1$  is an always-ascending direction if and only if it satisfies  $\nabla\sigma(p_c)^T L_\sigma^1(p_c, x) > 0$ , which is true since

$$\nabla\sigma(p_c)^T L_\sigma^1(p_c, x) = \frac{1}{ND^2} \sum_{i=1}^N |\nabla\sigma(p_c)^T x_i|^2$$

is positive if the deployment  $x$  spans  $\mathbb{R}^m$  and  $p_c \neq p_\sigma$ .  $\square$

Lemma 1 motivates us to analyze how  $L_\sigma^1$  (9) diverges from  $L_\sigma$  (8), the actual computed direction, concerning  $\|x\|$ .

**Lemma 2.** For a signal  $\sigma$ , a conservative divergence between  $L_\sigma^1(p_c, x)$  and  $L_\sigma(p_c, x)$  depends linearly on  $D$ , i.e.,

$$\|L_\sigma(p_c, x) - L_\sigma^1(p_c, x)\| \leq MD,$$

where  $M$  is the upper bound in (5).

*Proof.* From (6), (8) and (9), then it follows that

$$\begin{aligned} \|L_\sigma - L_\sigma^1\| &= \frac{1}{ND^2} \left\| \sum_{i=1}^N (\sigma(p_c + x_i) - \sigma(p_c) - \nabla\sigma(p_c)^T x_i) x_i \right\| \\ &\leq \frac{1}{ND^2} \sum_{i=1}^N M \|x_i\|^3 \leq MD. \end{aligned} \quad \square$$

*Remark 1.* Although it is not strictly necessary, we will aim to design deployments  $x$  such that  $L_\sigma^1$  is parallel to the gradient; this approach provides more flexibility to accommodate any deviation of  $L_\sigma$  from being an ascending direction.  $\blacktriangleleft$

Indeed, if  $D$  is small enough, then it is certain that  $L_\sigma$  is an ascending direction like  $L_\sigma^1$ . However, what is a *small*  $D$  for generic signals and deployments? Let us define  $E := L_\sigma - L_\sigma^1$ . Then we have  $\nabla\sigma(p_c)^T L_\sigma = \nabla\sigma(p_c)^T (L_\sigma^1 + E)$ , and let us consider a compact set  $\mathcal{S} \subset \mathbb{R}^m$  with  $p_\sigma \notin \mathcal{S}$ . By the definition of  $\sigma$  and its bounded gradient, we know that  $\nabla\sigma(p_c)^T L_\sigma^1$  has a minimum  $F_S(x)$  that depends on the chosen deployment  $x$  and it is positive if  $x$  is non-degenerate. Therefore, we have  $\nabla\sigma(p_c)^T L_\sigma \geq F_S(x) - K_S^{\max} M_S D$ , where  $K_S^{\max}$  and  $M_S$  are the maximum norms of the signal's gradient and Hessian in  $\mathcal{S}$ , respectively; thus, if

$$F_S(x) - K_S^{\max} M_S D > 0, \quad (10)$$

then  $L_\sigma$  is an ascending direction in  $\mathcal{S}$ . Finding the minimum  $F_S(x)$  numerically can be arduous so we will provide a more handy expression, but first we need the following result.

**Lemma 3.** If the deployment  $x$  is non-degenerate, then there exists  $C(x) > 0$  such that

$$\frac{1}{C(x)} \|\nabla\sigma(p_c)\|^2 \leq L_\sigma^1(p_c, x)^T \nabla\sigma(p_c) \leq C(x) \|\nabla\sigma(p_c)\|^2.$$

*Proof.* First, the trivial case  $\nabla\sigma(p_c) = 0$  satisfies the claim. In any other case, we know from Lemma 1 that  $\nabla\sigma(p_c)^T L_\sigma^1(p_c, x) = \frac{1}{ND^2} \sum_{i=1}^N |\nabla\sigma(p_c)^T x_i|^2 = \frac{1}{ND^2} \nabla\sigma(p_c)^T P(x) \nabla\sigma(p_c) > 0$  for the positive definite

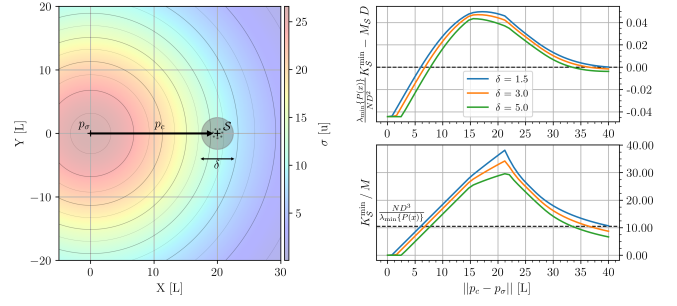


Fig. 3. Numerical illustration for Proposition 1. On the left, a radial scalar field  $\sigma(p) = \exp\{1\}$ . Within the grey circle, there is a deployment of seven robots with  $D = 0.75$  at the corners of a heptagon. On the right, above, we show for what sets  $\mathcal{S}$ , concerning  $\|p_c - p_\sigma\|$ , there is a sufficient guarantee for  $L_\sigma$  being an ascending direction within  $\mathcal{S}$ ; below, what is the ratio between the norms of the minimum gradient and maximum Hessian within  $\mathcal{S}$ .

matrix  $P(x) = \sum_{i=1}^N x_i x_i^T$  since  $x$  is non-degenerate. Therefore,

$$\frac{\lambda_{\min}\{P(x)\}}{ND^2} \|\nabla\sigma\|^2 \leq \nabla\sigma^T L_\sigma^1 \leq \frac{\lambda_{\max}\{P(x)\}}{ND^2} \|\nabla\sigma\|^2,$$

where  $\lambda_{\{\min, \max\}}\{P(x)\}$  are the minimum and maximum eigenvalues of  $P(x)$ , respectively. We choose  $C(x) = \max\{\frac{\lambda_{\max}\{P(x)\}}{ND^2}, \frac{ND^2}{\lambda_{\min}\{P(x)\}}\}$ .  $\square$

*Remark 2.* Although we will revisit the following known result within the context of our algorithm, it is well known that the eigenvalues  $\lambda\{P(x)\}$  of the covariance matrix are equal and positive for regular polygons/polyhedra deployments. Thus,  $\nabla\sigma^T L_\sigma^1 = \frac{\lambda_{\max}\{P(x)\}}{ND^2} \|\nabla\sigma\|^2$ .  $\blacktriangleleft$

Now, let us give an easier-to-check condition than (10).

**Proposition 1.** Let  $\mathcal{S}$  be a compact set with  $p_\sigma \notin \mathcal{S}$ . Then if

$$\frac{\lambda_{\min}\{P(x)\}}{ND^2} K_S^{\min} - M_S D > 0,$$

for  $\forall p_i \in \mathcal{S}$ , where  $K_S^{\min}$  is the minimum norm of the gradient in the compact set  $\mathcal{S}$ ,  $P(x) = \sum_{i=1}^N x_i x_i^T$ , then (8) is an ascending direction at  $p_c \in \mathcal{S}$ .

*Proof.* Since Lemma 3 lower bounds  $F_S(x)$  in (10) we have

$$\begin{aligned} \nabla\sigma(p_c)^T L_\sigma &= \nabla\sigma(p_c)^T L_\sigma^1 + \nabla\sigma(p_c)^T E \\ &= \frac{1}{ND^2} \nabla\sigma(p_c)^T P(x) \nabla\sigma(p_c) + \nabla\sigma(p_c)^T E \\ &\geq \frac{\lambda_{\min}\{P(x)\}}{ND^2} \|\nabla\sigma(p_c)\|^2 + \nabla\sigma(p_c)^T E, \end{aligned}$$

and to assess that  $L_\sigma(p_c)$  with  $p_c \in \mathcal{S}$  is an ascending direction is enough to check  $\frac{\lambda_{\min}\{P(x)\}}{ND^2} \|\nabla\sigma(p_c)\|^2 - \|\nabla\sigma(p_c)\| M_S D > 0$  or  $\frac{\lambda_{\min}\{P(x)\}}{ND^2} K_S^{\min} - M_S D > 0$ .  $\square$

*Example 1.* In Figure 3 we illustrate the result of Proposition 1. Given a symmetrical Gaussian signal with seven robots deployed at the corners of a regular heptagon with  $D = 0.75$ , we show for what balls  $\mathcal{S}$  around the swarm centroid  $p_c$  depending on the distance to the source are admissible to guarantee that  $L$  is an ascending direction.  $\blacktriangle$

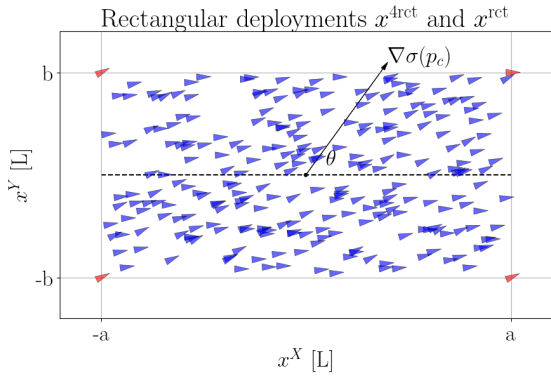


Fig. 4. The 4-robot rectangular deployment  $x^{4\text{rect}}$  are at the corners of the rectangle in red color. The 250 robots in blue color belong to the deployment  $x^{\text{rect}}$  and they are spread uniformly within the rectangle. The gradient  $\nabla\sigma(p_c)$  is arbitrary and forms an angle  $\theta$  with the horizontal axis of the deployment.

We note that the *covariance-like* matrix  $\frac{1}{N} \sum_{i=1}^N x_i x_i^T$  is normalized by  $D^2$  for checking the condition in Proposition 1, making the effective dependency on  $D$  linear and matching the result of Lemma 2.

While the signal  $\sigma$  is unknown, we can always engineer  $D$  depending on the expected scenarios. For example, in the scenario of contaminant leakage, scientists can provide the expected values of  $M_S$ ,  $K_S^{\max}$ , and  $K_S^{\min}$  in the *patrolling area*  $S$  for the minimum/maximum contamination thresholds where the robot team needs to react reliably. We also note that designing  $L_\sigma^1$  to be parallel to the gradient  $\nabla\sigma$  makes the scalar product  $\nabla\sigma^T L_\sigma > 0$  more robust concerning  $D$  since it makes admissible a larger deviation of  $L_\sigma$  from  $L_\sigma^1$ , e.g., misplaced robots from a reference deployment  $x$ .

As starting point to jump towards a *robot swarm*, let us first analyze the particular case when the robots are at the corners of regular polygons and polyhedra, and the sensitivity of the ascending direction when we *deform* such shapes. Let us consider four robots at the corners of a rectangle as deployment  $x^{4\text{rect}}$ , and assume that the long side of the rectangle is parallel to the horizontal axis so that the gradient  $\nabla\sigma(p_c) = \|\nabla\sigma(p_c)\| [\cos(\theta) \ \sin(\theta)]^T$  has an arbitrary norm and angle as depicted in Figure 4. Then, the always-ascending direction  $L_\sigma^1$  can be written as

$$L_\sigma^1(p_c, x^{4\text{rect}}) = \frac{\|\nabla\sigma(p_c)\|}{4D^2} \sum_{i=1}^4 \left( [\cos(\theta) \ \sin(\theta)] \begin{bmatrix} x_i^X \\ x_i^Y \end{bmatrix} \right) \begin{bmatrix} x_i^X \\ x_i^Y \end{bmatrix}, \quad (11)$$

where the superscripts  $X$  and  $Y$  denote the horizontal and vertical coordinates of  $x_i$  respectively. Therefore, for the deployment  $x^{4\text{rect}}$  we have that

$$\begin{aligned} L_\sigma^1(p_c, x^{4\text{rect}}) &= \frac{\|\nabla\sigma(p_c)\|}{4(a^2 + b^2)} \left( (a \cos(\theta) + b \sin(\theta)) \begin{bmatrix} a \\ b \end{bmatrix} + \right. \\ &+ (-a \cos(\theta) + b \sin(\theta)) \begin{bmatrix} -a \\ b \end{bmatrix} + (-a \cos(\theta) - b \sin(\theta)) \begin{bmatrix} -a \\ -b \end{bmatrix} + \\ &\left. + (a \cos(\theta) - b \sin(\theta)) \begin{bmatrix} a \\ -b \end{bmatrix} \right) = \frac{\|\nabla\sigma(p_c)\|}{(a^2 + b^2)} \begin{bmatrix} a^2 \cos(\theta) \\ b^2 \sin(\theta) \end{bmatrix}, \quad (12) \end{aligned}$$

where we can observe that if  $a$  or  $b$  equals zero, then only the projection of  $\nabla\sigma(p_c)$  onto the line described by the *degenerate*  $x$  in  $L_\sigma^1(p_c, x^{4\text{rect}})$  is observed. Nonetheless, let us

exploit such an *undesired* situation before coming back to the analysis of the rectangular deployment.

**Proposition 2.** Consider two degenerated and perpendicular segment deployments in 2D, i.e.,  $x^\parallel$  and  $x^\perp$  with  $N_\parallel$  and  $N_\perp$  numbers of robots, which are symmetrically distributed about their shared centroid. For both segments, in one semihalf, consider the farthest robot 1 from the centroid at the position  $a_1 \in \mathbb{R}^+$  and the rest  $i \in \{2, \dots, \frac{N}{2}\}$  at distances  $0 \leq a_{i+1} < a_i$  such that  $\sum_{i=2}^{\frac{N}{2}} a_i^2 = \frac{N}{4} a_1^2$ . If  $N$  is an odd number, then place one robot at the centroid, e.g.,  $a_0 = 0$ . Then,  $\lim_{N_\parallel \rightarrow \infty} L_\sigma^1(p_c, x^\parallel) + \lim_{N_\perp \rightarrow \infty} L_\sigma^1(p_c, x^\perp) = \frac{1}{2} \nabla\sigma(p_c)$ .

*Proof.* We first note that a robot at  $x_i = 0$  does not contribute at all; hence, since we require reflective symmetry around  $x = 0$  we can assume that  $N_\parallel$  and  $N_\perp$  are even so that their halves are also integer numbers. Looking at (9), we have that

$$L_\sigma^1(p_c, x^\parallel) = \frac{\|\nabla\sigma(p_c)\| \cos(\theta)}{N_\parallel a_1^2} 2 \sum_{i=1}^{\frac{N_\parallel}{2}} \begin{bmatrix} a_i^2 \\ 0 \end{bmatrix}.$$

Applying the condition  $\sum_{i=2}^{\frac{N}{2}} a_i^2 = \frac{N}{4} a_1^2$  from the statement, which can be checked feasible for a geometric series  $a_{i+1} = \alpha a_i$ ,  $i \in \{1, \dots, (\frac{N_\parallel}{2} - 1)\}$  for some  $0 < \alpha < 1$ , and  $a_{\frac{N_\parallel}{2}} = -\left(\sum_{i=2}^{\frac{N_\parallel}{2}-1} a_i^2 - \frac{N}{4}\right) < a_1^2$ , we have that

$$\begin{aligned} L_\sigma^1(p_c, x^\parallel) &= \frac{2\|\nabla\sigma(p_c)\| \cos(\theta)}{N_\parallel a_1^2} \begin{bmatrix} a_1^2 + \frac{N_\parallel}{4} a_1^2 & 0 \end{bmatrix}^T \\ &= \frac{1}{2} \|\nabla\sigma(p_c)\| \cos(\theta) \begin{bmatrix} \frac{4+N_\parallel}{N_\parallel} & 0 \end{bmatrix}^T. \end{aligned}$$

Similarly, we can arrive at  $L_\sigma^1(p_c, x^\perp) = \frac{1}{2} \|\nabla\sigma(p_c)\| \sin(\theta) \begin{bmatrix} 0 & \frac{4+N_\perp}{N_\perp} \end{bmatrix}^T$ . Thus, we have that  $\lim_{N_\parallel \rightarrow \infty} L_\sigma^1(p_c, x^\parallel) + \lim_{N_\perp \rightarrow \infty} L_\sigma^1(p_c, x^\perp) = \frac{1}{2} \nabla\sigma(p_c)$ .  $\square$

*Remark 3.* The geometric series for the distribution of the robots in Proposition 2 is only a suggestion but the sum  $\sum_{i=2}^{\frac{N}{2}} a_i^2 = \frac{N}{4} a_1^2$  gives us a hint about the importance of the second order moments of the robot distributions alongside both perpendicular axes. Indeed, if the variances of the two perpendicular *line-deployments* are equal then  $L_\sigma^1$  is parallel to the gradient. Note that the result from Proposition 2 tells us that amassing robots makes more robust the parallel estimation of the gradient. For example, if some individuals are missing or a bit misplaced then the variance of the deployment is less susceptible to be changed significantly.  $\blacktriangleleft$

As pointed after the Proposition 2 on having the same variance for the robot deployment in every axis, if we come back to (12) and consider the square  $a = b$  then we realize that  $L_\sigma^1(p_c, x^{4\text{rect}}) = \frac{1}{2} \nabla\sigma(p_c)$ . In fact, we show in the following technical result that  $L_\sigma^1(p_c, x^{N\text{poly}}) \propto [\cos\theta \ \sin\theta]^T$ , i.e., for any deployment  $x^{N\text{poly}}$  forming a regular polygon or polyhedron, then  $L_\sigma^1$  is parallel to the gradient  $\nabla\sigma(p_c)$ .

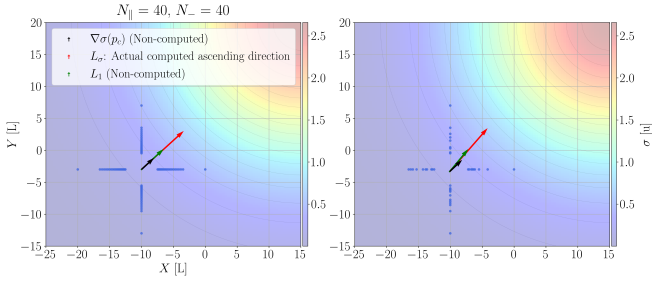


Fig. 5. Two *degenerated* crossed deployments as in Proposition 2 in the scalar field  $\sigma(p) = \frac{a}{\sqrt{2\pi s^2}} e^{-\frac{p_x^2 + p_y^2}{2s^2}}$ , with  $a = 1000$  and  $s = 15$ . On the left, the two variances are equal, hence  $L_1$  is parallel to the gradient and almost half of it (vectors represented at scale). On the right, we have removed randomly 20 agents in total from the four segments, and still we have an ascending direction for  $L_\sigma$ .

**Lemma 4.** Consider the deployment  $x^{Npoly}$  forming a regular polygon or polyhedron, and  $b \in \mathbb{R}^m$ , then

$$\sum_{i=1}^N (b^T x_i) x_i \propto b.$$

*Proof.* First, we have that  $\sum_{i=1}^N (b^T x_i) x_i = \sum_{i=1}^N (x_i x_i^T) b$ ; then, in order to be proportional to  $b$ , we need all the diagonal elements of the matrix  $P = \sum_{i=1}^N (x_i x_i^T)$  be equal and non-zero, and the non-diagonal to be zero. Since all the considered deployments lie on the  $(m-1)$ -sphere, all the  $\|x_i\|$  are equal. In addition, all the dihedral angles of the considered deployments are equal; then we can find XYZ axes where the set of all projections of the vertices  $x_i$  on the planes XY, XZ, and YZ, exhibit an even symmetry; hence,  $\sum_i (x_i^X)^2 = \sum_i (x_i^Y)^2 = \sum_i (x_i^Z)^2$ . Finally, a regular polygon has reflection symmetry for one axis of the same XY; hence,  $\sum_i (x_i^X)(x_i^Y) = 0$ . This is also true for a regular polyhedron for the same planes XY, XZ, and YZ.  $\square$

The geometrical interpretation of Lemma 4 is quite straightforward as well. If there is an equal distribution of robots alongside all the axes, e.g., the robots are at the vertices of a regular polygon, then the eigenvalues of their associated covariance matrix are all equal. From the fact that all the eigenvectors of the covariance matrix are orthogonal<sup>1</sup>, the claim of Lemma 4 follows. Note that we have arrived at the same conclusion as in [14], [15] but without an intensive usage of trigonometry for circular and spherical formations since regular polygons and polyhedra are inscribed in the circle and the sphere.

We now analyze the sensitivity of  $L_\sigma^1(p_c, x^{Npoly})$  when the deployment is under an affine transformation, e.g., scaling, rotation, and shearing. The formal affine transformation is given by  $(I_N \otimes A)x^{Npoly}$  with  $A \in \mathbb{R}^{m \times m}$  where  $A$  admits the Singular Value Decomposition (SVD)  $A = U\Sigma V^T$  describing a rotation, scaling, and another rotation.

<sup>1</sup>Note that if  $P$  is multiple of the identity matrix, the eigenvectors can be chosen orthogonal as well.

**Proposition 3.** Consider the deployment  $x^{Npoly}$  forming a regular polygon or polyhedron, and the SVD  $A = U\Sigma V^T$ , then

$$L_\sigma^1(p_c, (I_N \otimes A)x^{Npoly}) \propto U\Sigma^2 U^T r,$$

where  $r \in \mathbb{R}^m$  is the unitary vector marking the direction of the gradient  $\nabla\sigma(p_c)$ .

*Proof.* Considering the change of coordinates  $\tilde{r} = V\Sigma U^T r$

$$\begin{aligned} L_\sigma^1(p_c, (I_N \otimes (U\Sigma V^T))x^{Npoly}) &\propto \sum_{i=1}^N (r^T U\Sigma V^T x_i) U\Sigma V^T x_i \\ &\propto U\Sigma V^T \sum_{i=1}^N (\tilde{r}^T x_i) x_i \propto U\Sigma V^T \tilde{r} = U\Sigma V^T V\Sigma U^T r = U\Sigma^2 U^T r, \end{aligned}$$

where we have applied Lemma 4.  $\square$

Note that  $W = U\Sigma^2 U^T$  is the unitary decomposition of a positive definite matrix, and  $V$  is irrelevant, for example,  $\theta$  is arbitrary in 2D in Figure 4 as shown in Lemma 4. Stretching the deployment  $x^{Npoly}$  results in  $L_\sigma^1$  following the direction  $\xi \Sigma^2 \xi \nabla\sigma(p_c)$ , where  $\xi$  denotes the *stretching axes*. Such a morphing assists with maneuvering the swarm while it gets closer to the source.

The exploitation of symmetries does not stop with  $L_\sigma^1$ . Indeed, focusing on the second order of the Taylor series we have the following approximation

$$L_\sigma(p_c, x) \approx L_\sigma^0(p_c, x) + L_\sigma^1(p_c, x) + \frac{1}{ND^2} \sum_{i=1}^N \left( \frac{1}{2} x_i^T H_\sigma(p_c) x_i \right) x_i.$$

Following a similar notation, we can define

$$L_\sigma^2(p_c, x) := \frac{1}{ND^2} \sum_{i=1}^N \left( \frac{1}{2} x_i^T H_\sigma(p_c) x_i \right) x_i.$$

It is straightforward to see that  $L_\sigma^2(p_c, x) = 0$  for certain deployments like an even distribution such as  $x^{A_{rect}}$ .

**Proposition 4.**  $L_\sigma(p_c, x) = L_\sigma^1(p_c, x)$  for deployments with even symmetries in quadratic scalar fields.

*Proof.* Consider a quadratic scalar field  $\sigma(p) = b^T p + \frac{1}{2} p^T H p$ , and place the barycenter of the deployment at a generic point  $\xi = (p - a)$ . Then, we have that  $\sigma(\xi) = \underbrace{b^T a + 0.5 a^T H a}_{\sigma(p=a)} + \underbrace{(b^T + a^T H) \xi + \frac{1}{2} \xi^T H \xi}_{\tilde{b}^T \xi}$ . Consequently, for an even deployment we have that  $L_\sigma(p_c, x) = L_\sigma^1(p_c, x) = \frac{P}{ND^2} \tilde{b}$  with  $P$  as the covariance of the deployment as in Lemma 4.  $\square$

While simple, quadratic scalar fields as in Proposition 4 has a direct relation with signal models that are very present in the physical world, such as the logarithm of Gaussian fields or the inverse of  $\frac{1}{r^2}$  laws, as mentioned in the Introduction.

### B. Continuous distributions of robots

Looking at the definition of  $L_\sigma$  in (8), it is clear that we can apply the superposition of many, potentially infinite, deployments. Indeed, we can jump into *continuous* deployments considering  $N \rightarrow \infty$  within a specific area or volume. In such a case, the finite sum in (8) becomes

an integral with a robot density function following the approximation of a definite integral with Riemann sums. In order to keep a consistency with the units,  $ND^2$  in (8) becomes  $A = \iiint_{\mathcal{A}} \rho(X, Y, Z) dXdYdZ$ , where  $\mathcal{A}$  is the corresponding surface/volume within the perimeter delimited by  $x$ , and  $\rho : \mathcal{A} \rightarrow \mathbb{R}^+$  is a normalized (robot) density function, e.g., equal everywhere in  $\mathcal{A}$  for uniform distributions as it is shown in Figure 4 with  $x^{rct}$ . Note that  $A$  will be irrelevant for our algorithm since we are only interested in the direction of the *ascending direction* and not in its norm.

For the sake of conciseness, let us focus on 2D for the following results, and for the sake of clarity with the notation, we will denote  $x_i^X$  and  $x_i^Y$  as simply  $X$  and  $Y$ . Accordingly, for the case of a swarm described by a density function  $\rho(X, Y)$  of robots within a generic shape/surface  $\mathcal{A}$ , the always-ascending direction can be calculated as

$$\begin{aligned} L_{\sigma}^1(p_c, x) &= \frac{\|\nabla\sigma(p_c)\|}{A} \iint_{\mathcal{A}} \rho(X, Y) \begin{bmatrix} \cos(\theta) & \sin(\theta) \end{bmatrix} \begin{bmatrix} X \\ Y \end{bmatrix} \begin{bmatrix} X \\ Y \end{bmatrix} dXdY \\ &= \frac{\|\nabla\sigma(p_c)\|}{A} \iint_{\mathcal{A}} \rho(X, Y) \begin{bmatrix} X^2 \cos(\theta) + XY \sin(\theta) \\ Y^2 \sin(\theta) + XY \cos(\theta) \end{bmatrix} dXdY. \end{aligned}$$

Similar to the discrete case, e.g., see (12), it is enough to have  $\iint_{\mathcal{A}} \rho(X, Y) XY dXdY$  and  $\iint_{\mathcal{A}} \rho(X, Y) (X^2 - Y^2) dXdY$  equal to zero to have  $L_{\sigma}^1$  parallel to the gradient.

**Proposition 5.** Consider a signal  $\sigma$ , a continuous deployment  $x$  with robot density function  $\rho(X, Y)$  within an area  $\mathcal{A}$ , and a Cartesian coordinate system  $(X - Y)$  with origin at the centroid of the deployment  $p_c$ . The direction of  $L_{\sigma}^1(p_c, x)$  is parallel to the gradient  $\nabla\sigma(p_c)$  if  $\rho(X, Y)$  and  $\mathcal{A}$  hold the following symmetries:

- S0) The robot density function  $\rho(X, Y)$  has reflection symmetry (even function) concerning at least one of the axes  $(X - Y)$ , e.g.,  $\rho(X, Y) = \rho(-X, Y)$ .
- S1) The surface  $\mathcal{A}$  has reflection symmetry concerning the same axes as in S0.
- S2) For each quadrant of  $(X - Y)$ , the robot density function  $\rho(X, Y)$  has reflection symmetry concerning the bisector of the quadrant.
- S3) The surface  $\mathcal{A}$  has reflection symmetry concerning the same axes as in S2.

*Proof.* Without loss of generality, we assume that the reflection symmetry is on the  $Y$  axis, and we assume symmetric integration limits for the horizontal axis as in Figure 6(a). First, if  $\alpha(X)$  and  $\beta(X)$  are both even functions as illustrated in Figure 6(a), we are going to show that

$$\begin{aligned} \iint_{\mathcal{A}} \rho(X, Y) XY dXdY &= \\ \int_{-t_{\beta}}^{t_{\beta}} \int_0^{\beta(X)} \rho(X, Y) XY dXdY + \int_{-t_{\alpha}}^{t_{\alpha}} \int_{\alpha(X)}^0 \rho(X, Y) XY dXdY \\ &= \int_{-t_{\beta}}^{t_{\beta}} XF(X, \beta(X)) dX - \int_{-t_{\alpha}}^{t_{\alpha}} XF(X, \alpha(X)) dX = 0, \end{aligned} \quad (13)$$

where  $F(X, Y) = \int \rho(X, Y) Y dY$ . Given an arbitrary even function  $f(X)$  and knowing that  $\rho(X, Y) = \rho(-X, Y)$ , we have that  $F(X, Y) = F(-X, Y)$  and  $F(X, Y) = F(X, f(X)) = F(-X, f(-X)) = F(X, -Y)$ ; therefore, both integrals in (13) are zero considering symmetries  $S\{0,1\}$ .

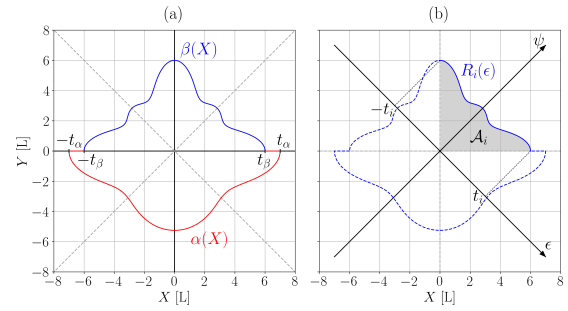


Fig. 6. Illustration of the symmetries  $S\{1,3\}$  for the surface  $\mathcal{A}$  on the left and right respectively, to design  $L_{\sigma}^1(p_c, x)$  parallel to the gradient  $\nabla\sigma(p_c)$ .

Next, we will divide  $\mathcal{A}$  into four parts for each quadrant, as it is shown in Figure 6(b), so that

$$\iint_{\mathcal{A}} \rho(X, Y) (X^2 - Y^2) dXdY = \sum_{i=1}^4 \iint_{\mathcal{A}_i} \rho(X, Y) (X^2 - Y^2) dXdY,$$

where  $\mathcal{A}_i$  is the area of the quadrant  $i \in \{1, 2, 3, 4\}$ . From the symmetry exhibited by  $X^2 - Y^2$  we propose the following change of variables  $g(\epsilon, \psi) = (\psi + \epsilon, \psi - \epsilon)/\sqrt{2}$ , which is equivalent to a rotation of  $-\pi/4$  radians for the  $(X - Y)$  axes. Since  $\int_{\mathcal{A}} f(x, y) = \int_{\mathcal{B}} (f \circ g) |J_g|$ , where  $|J_g| = |\begin{bmatrix} \nabla g_1 & \nabla g_2 \end{bmatrix}^T| = \sqrt{2}$ , we have

$$\begin{aligned} \iint_{\mathcal{A}_i} \rho(X, Y) (X^2 - Y^2) dXdY &= 2\sqrt{2} \iint_{\mathcal{B}_i} \rho(\epsilon, \psi) \epsilon\psi d\epsilon d\psi \\ &= 2\sqrt{2} \int_{-t_i}^{t_i} \int_{|\epsilon|}^{R_i(\epsilon)} \rho(\epsilon, \psi) \epsilon\psi d\epsilon d\psi = 2\sqrt{2} \int_{-t_i}^{t_i} \epsilon [F(\epsilon, R_i(\epsilon)) - F(\epsilon, |\epsilon|)] d\epsilon, \end{aligned}$$

which is zero if  $R_i(\epsilon) = R_i(-\epsilon)$  for all quadrants since  $|\epsilon|$  is an even function. Such condition is satisfied if  $\alpha(X)$  and  $\beta(X)$  have reflection symmetry concerning the bisector of the two lower and upper quadrants respectively as illustrated in Figure 6(b); thus, symmetries  $S\{2,3\}$  are checked.  $\square$

Indeed, not only *uniform* deployments  $x^{\text{Upoly}}$  describing an area/volume of a regular polygon/polyhedron fit into Proposition 5, but a richer collection of deployments like the ones depicted in Figures 6 and 7. In fact, if only  $S\{0,1\}$  are satisfied, by focusing on  $\rho(X, Y)$  and its variances  $\text{VAR}_{\mathcal{A}}[X] \neq \text{VAR}_{\mathcal{A}}[Y]$  we have that

$$L_{\sigma}^1(p_c, x) = \frac{\|\nabla\sigma(p_c)\|}{A} \begin{bmatrix} \text{VAR}_{\mathcal{A}}[X] \cos(\theta) \\ \text{VAR}_{\mathcal{A}}[Y] \sin(\theta) \end{bmatrix},$$

where the relation between variances *maneuvers* the swarm while getting closer to the source, as it is shown in Figure 8.

#### IV. DISTRIBUTED ARCHITECTURE OF THE PROPOSED SOURCE-SEEKING SYSTEM

So far, our methodology would require a central robot which collects all the  $\sigma(p_c + x_i)x_i$  and computes  $L_{\sigma}$  as in (8); meaning that the entire robot swarm becomes non-operational if such computing robot serving as a nexus disappears. While assigning backup computing robots could be a solution, an alternative approach is to estimate all kind of required information distributively. The main idea is to



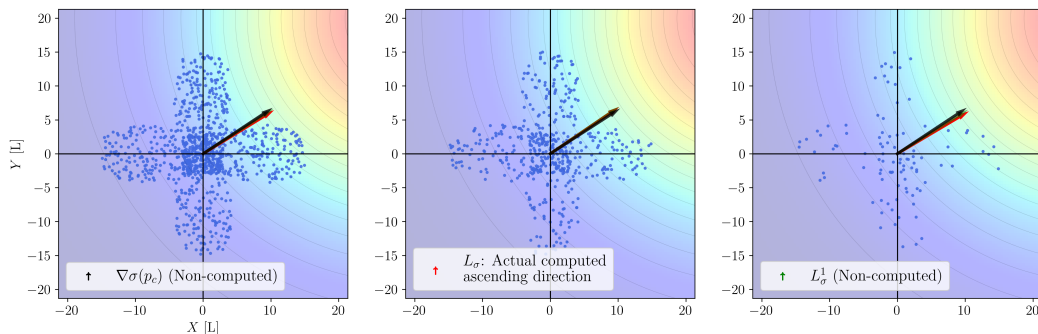


Fig. 7. On the left, a swarm of 1000 robots satisfying the symmetries  $S\{0, 1, 2, 3\}$  from Proposition 5. For the three figures, the black arrows are the gradient  $\nabla\sigma$ , the green arrows are  $L_\sigma^1$ , and the red arrows are the direction  $L_\sigma$  computed by the robots. Arrows are normalized for representation purposes as we focus only on their direction. As we get far from *the continuum*, with 500 and 100 robots on the middle and right figures, there is no guarantee that  $L_\sigma^1$  is parallel to the gradient  $\nabla\sigma$ . However, in this example,  $L_\sigma$  has almost the same direction as  $L_\sigma^1$  despite a *big D* concerning the level curves.

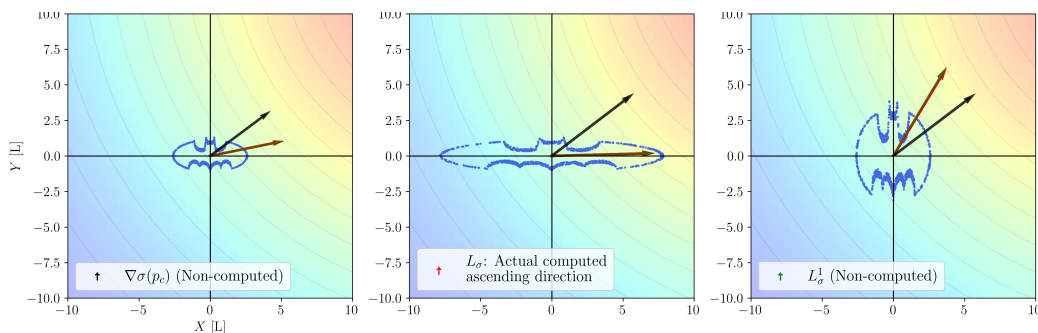


Fig. 8. On the left, a swarm of 1000 robots satisfying only the symmetries  $S\{0, 1\}$  from Proposition 5. The arrows have the same meaning as in Figure 7. The modification of the variances of  $\rho(X, Y)$ , e.g., by stretching the swarm shape, stretches  $L_\sigma^1$  and  $L_\sigma$  accordingly. In this example, the direction of  $L_\sigma$  almost does not diverge from  $L_\sigma^1$  despite a *big D* concerning the level curves.

enhance further the resilience of the robot swarm with a distributed architecture with no leaders and where individuals can join and leave the swarm in the middle of the mission.

In order to provide a self-contained and distributed source-seeking solution, we show the following items in the upcoming subsections:

- Compatibility of the source-seeking solution with a displacement-based formation controller.
- Distributed estimation of the swarm centroid, i.e., each robot needs to estimate its corresponding  $x_i$  in (8).
- Distributed calculation of the ascending direction (8).

We illustrate the system architecture in Figure 9. Note that the last two items of the list must happen sequentially since  $x_i$  is necessary to estimate the direction of  $L_\sigma$ , and the formation control can run simultaneously with the tracking of the ascending direction. The tracking controllers will be shown in the upcoming Sections V and VI.

#### A. Displacement-based formation control

We briefly discuss how certain properties of a standard displacement-based formation controller can be leveraged with our source-seeking algorithm, particularly for single integrator dynamics. In particular, this briefing will help us introduce our algorithm for the centroid estimator.

We have seen in Lemma 4 that the calculation of the ascending direction  $L_\sigma$  can be assisted with a convenient

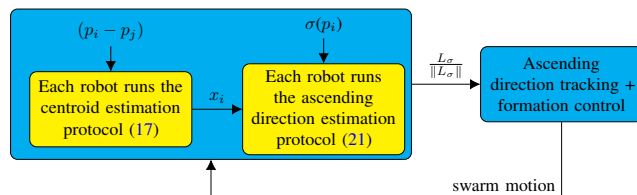


Fig. 9. System architecture showing all the algorithms and inputs/outputs involved in the proposed source-seeking solution. The two blue boxes run in parallel simultaneously. The yellow boxes represent the distributed estimators of the swarm centroid and the ascending direction, which operate sequentially. A new ascending direction is provided to the tracking controller at a fixed frequency. Therefore, the two estimators are reset at a sufficiently fast frequency, ensuring a minimum time required to assess the local values and converge close enough to the consensus. For example, their reset time can be determined by the algebraic connectivity of a synchronized network. Sufficiently fast means that the relative positions and the measurement of the signal can be considered constant until a new ascending direction  $\frac{L_\sigma}{\|L_\sigma\|}$  is provided, e.g., the robots move slow enough concerning the scalar field.

robot deployment  $x$ . If robots can measure or determine their relative positions, then the following control action for the single integrator (3)

$$u_i^f = - \sum_{j \in \mathcal{N}_i} (p_i - p_j) - (p_i^* - p_j^*), \forall i \in \mathcal{V}, \quad (14)$$

drives all robots to their desired relative positions  $(p_i^* - p_j^*)$  [33]. The work presented in [34] analyzes the explicit solution of (14), and its practical implications involving realistic

positioning sensors. In particular, the compact form of (14) can be written as

$$u^f = -\bar{L}(p - p^*), \quad (15)$$

where  $u^f \in \mathbb{R}^{mN}$  is the stacked vector of control actions  $u_i^f$  and  $p^*$  is the desired deployment with respect to an arbitrary fixed reference frame, and  $L$  is the Laplacian matrix (2), possibly sharing the network topology used in (21). Note that the robots will not converge to the actual  $p^*$ , but as analyzed in [34], to a point  $p \in \mathcal{P} := \{p : p = p^* + (\mathbf{1}_n \otimes c), c \in \mathbb{R}^m\}$ ; i.e., what is important is that  $\lim_{t \rightarrow \infty} p(t) \in \mathcal{P}$  has the required *shape*. In fact, if the desired shape  $p^*$  is written with respect to  $p_c$ , then  $\lim_{t \rightarrow \infty} x(t) = p^*$  exponentially fast [34]. In particular, the vector  $\mathbf{1}_N$  spans the kernel space of  $L$ ; therefore, having all the robots following the common velocity  $\frac{L_\sigma}{\|L_\sigma\|}$ , in addition to  $u^f$ , will not interfere with the formation control action, i.e.,  $\bar{L} \left( \mathbf{1}_N \otimes \frac{L_\sigma}{\|L_\sigma\|} \right) = 0$ . In fact,  $u^f$  keeps the centroid of  $x$  invariant since  $\sum_{i=1}^N u_i^f = 0$  since  $\mathbf{1}_m^T L = 0$  because of (2) and  $B^T \mathbf{1}_N = 0$ . Hence, we propose for single-integrator robots to track, in compact form, the following velocity

$$u = \left( \mathbf{1}_N \otimes \frac{L_\sigma}{\|L_\sigma\|} \right) + u^f, \quad (16)$$

whose tracking analysis in Section V will solve Problem 1.

### B. Distributed estimation of the centroid

We continue with the algorithm that estimates the necessary barycentric coordinates  $x_i$  distributively. The proposed algorithm emerges from a collection of well-established results from formation control. In particular, the formation control problem has its dual in the relative localization problem [33], [35]. We first note that in (15) the *software* term  $\bar{L}p^*$  defining the desired formation is fixed, while the *hardware* term associated with the robot measurements  $\bar{L}p$  is dynamic, i.e., the formation control action  $u^f$  actuates over the velocities/positions of the robots  $p$ . Now, consider the *dual dynamics* of (15)

$$\frac{d}{dt} \hat{x}_i(t) = - \sum_{j \in \mathcal{N}_i} \left( (\hat{x}_i(t) - \hat{x}_j(t)) - (x_i - x_j) \right), \forall i \in \mathcal{V}, \quad (17)$$

where the network topology can be the same as before in (15), but now the fixed term is the *hardware* measurement  $(x_i - x_j)$ , which is equivalent to the relative position  $(p_i - p_j)$ , and the dynamic term is the *software* estimation  $\hat{x}_i \in \mathbb{R}^m$ , i.e., the estimation of the position of the centroid from the robot  $i$ . Note that since  $\hat{x}_j$  is a software value, then it needs to be communicated to robot  $i$  for all  $(i, j) \in \mathcal{E}$ .

**Proposition 6.** *The estimation  $\hat{x}_i$  in (17) converges exponentially fast to the actual  $x_i$  as  $t \rightarrow \infty$  if and only if  $\sum_{i=1}^N \hat{x}_i(0) = 0$ .*

*Proof.* We first recall that the considered type of graph for the following results is undirected and connected.

Let us write the compact form of (17) as

$$\begin{aligned} \frac{d}{dt} \hat{x}(t) &= -\bar{L}\hat{x}(t) + \bar{L}x \\ \frac{d}{dt} \hat{x}(t) + \bar{L}\hat{x}(t) &= \delta, \end{aligned} \quad (18)$$

where here  $L$  is the Laplacian matrix (2) again so that  $\delta = \bar{L}x = \bar{L}p \in \mathbb{R}^{m|\mathcal{E}|}$  is the stacked vector of relative positions  $(x_i - x_j) = (p_i - p_j)$ ,  $(i, j) \in \mathcal{E}$ . We note that the dynamics of  $\sum_{i=1}^N \hat{x}_i(t)$  are stationary, i.e.,  $\sum_{i=1}^N \frac{d}{dt} \hat{x}_i(t) = 0$  since

$$\mathbf{1}_{mN}^T (-\bar{L}\hat{x}(t) + \bar{L}x) = 0, \quad (19)$$

in view of (2) and  $B^T \mathbf{1}_N = 0$ . Hence, if  $\sum_{i=1}^N \hat{x}_i(0) = 0$ , the centroid or average of  $\hat{x}(t)$  will remain at zero  $\forall t$ . Note that this is a sufficient and also necessary condition for the invariance of the centroid of  $\hat{x}(t)$  since  $\mathbf{1}_N^T$  is the only left eigenvector of  $L$  associated with its single zero eigenvalue. We also know that the eventual trajectory  $\hat{x}^h(t)$  of the homogeneous part of the differential equation (18) is given by

$$\lim_{t \rightarrow \infty} \hat{x}^h(t) = \mathbf{1}_N \otimes c_1, \quad (20)$$

since  $\mathbf{1}_N$  is the eigenvector associated to the single eigenvalue zero of  $L$ ,  $c_1 \in \mathbb{R}^m$  is up to the initial condition  $\hat{x}(0)$ , and the rest of terms of  $\hat{x}^h(t)$  vanish exponentially fast since  $L$  is positive semidefinite<sup>2</sup>.

We can check that  $\hat{x}^p = x + (\mathbf{1}_N \otimes c_2)$  is a family of particular solutions for (18), where  $c_2 \in \mathbb{R}^m$ , since  $\bar{L}\hat{x}^p = \delta$ ; thus,

$$\lim_{t \rightarrow \infty} \hat{x}(t) = \left( \mathbf{1}_N \otimes (c_1 + c_2) \right) + x.$$

However, since the centroid of  $x$  is zero by definition, and the centroid of  $\hat{x}(0)$  is assumed to be zero and it is invariant because of (19), it must be true that  $(c_1 + c_2) = 0$ , i.e.,  $x$  and  $\hat{x}(t)$  share the same frame of coordinates; therefore,  $\lim_{t \rightarrow \infty} \hat{x}(t) = x$ , exponentially fast.  $\square$

*Remark 4.* The condition  $\sum_{i=1}^N \hat{x}_i(0) = 0$  can be satisfied by setting all the initial software values  $\hat{x}_i(0) = 0$ .  $\blacktriangleleft$

### C. Distributed calculation of the ascending direction

A standard consensus algorithm [27, Chapter 7] can be exploited to estimate the direction of the vector  $L_\sigma$  as in (8). As we will see later, the robot swarm will track the direction of  $L_\sigma$  while traveling at a constant speed. Indeed,  $N$  and  $D^2$  are not necessary to know the direction of  $L_\sigma$  but by defining  $\mu := 1N \sum_{i=1}^N \sigma(p_c + x_i)x_i$  then we have that  $\hat{L}_\sigma := \frac{L_\sigma}{\|L_\sigma\|}$  and  $\hat{\mu} := \frac{\mu}{\|\mu\|}$  are equal. Hence, if we set  $\mu_i(0) = \sigma(p_c(0) + x_i(0))x_i(0)$ , we have that  $\lim_{t \rightarrow \infty} \mu_i(t) \rightarrow \mu$  exponentially fast if a connected network within the robot swarm follows the consensus protocol

$$\begin{cases} \dot{\mu}_i(t) &= \sum_{j \in \mathcal{N}_i} (\mu_j(t) - \mu_i(t)), \forall i \in \mathcal{V}. \\ \mu_i(0) &= \sigma(p_c(0) + x_i(0))x_i(0), \end{cases} \quad (21)$$

<sup>2</sup>In fact, we know that  $c_1 = \frac{1}{N} \left( \sum_{i=1}^N \hat{x}_i(0) \right)$  [36] since we follow a standard consensus protocol, but this result is not necessary for our analysis.

Indeed,  $\mu(t)$  is not meant to evolve with  $x(t)$  and  $p_c(t)$  but the consensus protocol (21) runs sequentially after running (17) so that all the  $\hat{x}_i(t)$  have been set. The system has to reset the protocol (21), and also (17) consequently, for a *new round* once the robots have approached  $\mu$ . We recall that since the convergence to  $\mu$  happens exponentially fast, if the network topology is known, its algebraic connectivity  $\lambda_2$  [27] can be used to reset (21), and it can be further tuned with a positive gain  $k_\mu$  in (21), e.g., the robots achieve around the 99% of  $\mu$  after  $\frac{k_\mu}{\lambda_2}$  time units. We highlight that the speed of the robots is independent of the estimation of  $\mu$  since the speed is an independent parameter. If robots travel slow enough we can assume safely that  $\sigma(p_i)$  and  $x_i$  are almost constant while the protocol (21) produces a new ascending direction to be tracked.

## V. SOURCE-SEEKING WITH SINGLE-INTEGRATOR ROBOTS

Focusing on robots with the single-integrator dynamics (3), we will show formally that the direction of  $L_\sigma(p_c(t), x)$  can guide the centroid of the robot swarm to the signal source effectively while running a displacement-based formation control algorithm. In order to be concise, the following theorem assumes that both, the barycentric coordinates  $x_i$  and the ascending direction  $\frac{L_\sigma(p_c(t), x)}{\|L_\sigma(p_c(t), x)\|}$  are available to all the robots instantaneously. In practice, since such information is estimated exponentially fast, we can assume the estimated but very close values to the actual ones as experiencing small disturbances to the *perfect* system.

**Theorem 1.** *Consider the signal  $\sigma$  and a swarm of  $N$  robots with the stacked positions  $p(t) \in \mathbb{R}^{mN}$ , where  $m = \{2, 3\}$ . Assume that  $x^*$  is not degenerated, and the initial deployment  $x(0) = x^* + \delta$  is within a compact set with  $\delta \in \mathbb{R}^{mN}$ ,  $\|\delta\| \leq \Delta \in \mathbb{R}^+$  and also not degenerate. Then*

$$\begin{cases} \dot{p}_i(t) &= \frac{L_\sigma(p_c(t), x(t))}{\|L_\sigma(p_c(t), x(t))\|} - \sum_{j \in \mathcal{N}_i} (x_i - x_j) - (x_i^* - x_j^*) \\ p_i(0) &= p_c(0) + x_i^* + \delta_i, \quad p_c \neq p_\sigma, \delta_i \in \mathbb{R}^m, \end{cases} \quad (22)$$

is a solution to Problem 1 given the conditions of Proposition 1 for an annulus shell  $\mathcal{S}$  around  $p_\sigma$ .

*Proof.* We first consider the dynamics of the following system

$$\begin{cases} \dot{p}_i(t) &= L_\sigma^1(p_c(t), x(t)) - \sum_{j \in \mathcal{N}_i} (x_i - x_j) - (x_i^* - x_j^*) \\ p_i(0) &= p_c(0) + x_i^* + \delta_i, \quad p_c \neq p_\sigma, \delta_i \in \mathbb{R}^m, \end{cases} \quad (23)$$

and afterward we continue to analyze the system (22) in the statement. We note that the dynamics of  $p_c(t)$  are  $\dot{p}_c(t) = L_\sigma^1(p_c(t), x(t))$  because  $1_{mN}^T \bar{B} \bar{B}^T (x(t) - x^*) = 0$ , i.e., the displacement-based formation controller does not change the centroid as it was detailed in Subsection IV-A.

Let us consider the function  $\sigma(p_c(t))$ , and without loss of generality, let us set the maximum  $p_\sigma$  at the origin so that  $\sigma(p) \rightarrow \sup\{\sigma\} = \sigma(0)$  as  $\|p\| \rightarrow 0$ , and  $\sigma(p) \rightarrow 0$  as  $\|p\| \rightarrow \infty$ . Because of Definition 2,  $\sigma(p)$  does not have any local minima but only the global maximum  $\sup\{\sigma\} = \sigma(0)$ . The dynamics of  $\sigma(p_c(t))$  under (23) is:

$$\dot{\sigma}(p_c(t)) = \nabla \sigma(p_c)^T \dot{p}_c(t) = \nabla \sigma(p_c)^T L_\sigma^1(p_c(t), x(t)) \geq 0,$$

and if  $x(t)$  is not degenerated for all  $t$ , then the equality holds if and only if  $p_c = p_\sigma$  because of Lemma 1. The deployment  $x(t)$  is not degenerated since  $x(0) = x^* + \delta$  is not degenerated and  $x(t)$  is within a non-degenerated compact set converging exponentially fast to  $x^*$  as  $t \rightarrow \infty$ .

Let us consider the Lyapunov function  $V = (\sigma(p_c(t)) - \sigma(0))^2/2$ , and calculating the time derivative with respect to (23), we have

$$\begin{aligned} \dot{V}(t) &= (\sigma(p_c(t)) - \sigma(0)) \nabla \sigma^T(p_c(t)) \dot{p}_c(t) \\ &= \underbrace{(\sigma(p_c(t)) - \sigma(0)) \nabla \sigma^T(p_c(t)) L_\sigma^1(p_c(t), x(t))}_{W(t)} \leq 0. \end{aligned}$$

At this point, we can invoke LaSalle's invariance principle to conclude that  $W(t) \rightarrow 0$  as  $t \rightarrow \infty$ ; or equivalently  $\lim_{t \rightarrow \infty} p_c(t) = p_\sigma = 0$  since we recall that  $x(t)$  is not degenerate. Therefore, given an  $\epsilon > 0$ , there is always a time  $T^* > 0$ , such that  $\|p_c(t) - p_\sigma\| < \epsilon, \forall t > T^*$ , as first required to solve the source-seeking Problem 1.

Let us focus now on the system (22). We first know that  $\frac{L_\sigma(p_c(t), x(t))}{\|L_\sigma(p_c(t), x(t))\|}$  is well defined in  $\mathcal{S}$  if  $x(t)$  is not degenerate. Let us consider the annulus shell  $\mathcal{S}$  centered at  $p_\sigma$  and with radii  $\epsilon^+ > \epsilon_- > 0$ , then, according to Proposition 1, there exists  $D^*(\epsilon^+, \epsilon_-)$  such that if  $D \leq D^*$  the trajectory of  $p_c(t)$  under the dynamics (22) is an ascending one so that we can apply the same arguments as for the system (22) and solve the source-seeking Problem 1 where its  $\epsilon = \epsilon_-$  and the initial condition must satisfy  $\|p_c(0)\| \leq \epsilon^+$ . For all  $t > T^*$  such that  $\|p_c(T^*) - p_\sigma\| < \epsilon_-$ , we note that since the robots have single integrator dynamics, if the centroid of the swarm comes back to the compact set  $\mathcal{S}$  it will only stay at its closure and leave it again since  $L_\sigma$  is an ascending direction at the closure of  $\mathcal{S}$ . If  $L_\sigma$  turns out to be zero outside of  $\mathcal{S}$  then the swarm can stop.  $\square$

## VI. SOURCE-SEEKING WITH CONSTANT-SPEED UNICYCLE ROBOTS

### A. Guiding vector field

We continue our analysis when the robot swarm consists of 3D unicycle robots with constant speed modelled as in (4). While  $L_\sigma(p_c, x)$  is technically the guiding vector of the robot swarm, there are two main differences with respect to other guiding vector fields [9], [10], [37]. Firstly, the field constructed from  $L_\sigma(p_c, x)$  not only depends on the point  $p_c$  of the three dimensional space but also on the deployment  $x$ , which is not constant in general during the initial time. During a such transitory, the centroid  $p_c$  could be deviated from tracking the desired direction. Secondly, since the signal  $\sigma$  is unknown, the robot swarm does not know the rate of change of  $L_\sigma(p_c, x)$  throughout the field, and therefore it cannot be compensated with a feed-forward term for the control action  $\Omega_i$  in (4) as it is done in [9], [10], [37]. We will follow a similar strategy as in the proof of Theorem 1, i.e., we will consider first the always-ascending  $L_\sigma^1(p, x)$  for the analysis and afterward we analyze a worst case scenario considering  $L_\sigma(p, x)$  as a bounded deviation from the ideal direction  $L_\sigma^1(p, x)$ . It is important to note that we seek the

alignment of the  $X$ -axis of the unicycle robots with the ascending direction, i.e., we leave *free* the alignment of the other two axis, e.g., they can be assigned to a known rotational velocity as we will see in the analysis and simulations.

### B. Geometric controller for aligning the unicycle robot to a vector field with an unknown time variation

Following the spirit of [29] for roboticists, we have derived in a detailed way in [30] all the (well-known) concepts and techniques from geometric control that are necessary for our results, e.g., how to exploit geodesics for the 3D attitude control to track a vector field. In the following of this subsection, let us review such necessary technicalities.

Consider a set  $U \subset \mathbb{R}^{3N}$  where  $L_\sigma^1(p, x) \neq 0$ , and define  $m_d : U \rightarrow \mathbb{R}^3$

$$m_d(p) = \frac{L_\sigma^1(p)}{\|L_\sigma^1(p)\|}, \quad (24)$$

so that we construct a *target attitude matrix*

$$R_a(p) := [m_d(p) \ y_a \ z_a] \in \text{SO}(3), \quad (25)$$

where  $\{m_d(p), y_a, z_a\}$  is an orthonormal basis of  $\mathbb{R}^3$ . Our objective now is to align as close as possible the heading direction of our 3D unicycle robots, i.e.,  $\hat{p}_i := \dot{p}_i / \|\dot{p}_i\|$ , with  $m_d(p)$ . Recalling that the velocity of the robots in their body frame is  $[1 \ 0 \ 0]^\top$  and their attitude matrix  $R(t) = [R_x \ R_y \ R_z]$  with  $\{R_x, R_y, R_z\}$  being an orthonormal basis of  $\mathbb{R}^3$ ; then, the alignment of the robots with (24) happens when  $\hat{p}_i^\top R_x = 1$ , and  $\hat{p}_i^\top R_y = \hat{p}_i^\top R_z = 0$ . This problem is equivalent to minimize the geodesic distance in  $S^2 := \{a \in \mathbb{R}^3 \mid \|a\| = 1\}$  [28]

$$d_{S^2}(x, y) = \arccos(x^\top y), \quad (26)$$

where  $\arccos(\cdot)$  takes values between 0 and  $\pi$ , between  $R_x(t)$  and  $m_d(p(t))$ .

If we know  $R_a$  and  $\dot{R}_a$ , it is possible to align asymptotically the unicycle's attitude  $R$  with  $R_a$  by following the next control law for (4)

$$\Omega(R_e) = -k_w \log(R_a^\top R) + R^\top \dot{R}_a R_a^\top R, \quad (27)$$

where the first term is a proportional controller and the second one is the feed-forward anticipating the change of the target attitude. In fact, the controller (27) makes it possible to drive the following geodesic distance in  $\text{SO}(3)$

$$\mu_{R_e} := d_{\text{SO}(3)}(R_a, R) = \|\log(R_e)\|_F, \quad (28)$$

exponentially fast to zero if  $\text{tr}(R_e(t_0)) \neq -1$ , where  $R_e = R_a^\top R$  [28], [30]. We also note that the feed-forward term in (27) can be identified with the *adjoint* map as  $R^\top \dot{R}_a R_a^\top R = \text{Ad}_{R_e^\top}(\Omega_a) = R_e^\top \Omega_a R_e$  [28], [30] so we only need to employ the desired angular velocities coming from the desired target attitude to calculate the feed-forward term of (27).

Indeed, we have certain freedom in assigning  $y_a$  and  $z_a$  in (25) but we do not know how  $m_d(p(t))$  evolves. Let us split the *target angular velocity* into

$$\Omega_a = \Omega_a^u + \Omega_a^k, \quad (29)$$

where  $\Omega_a^u$  is an unknown variation of  $R_a(t)$  associated to the time variation of  $m_d(t)$  and  $\Omega_a^k$  can be configured through the design of the, possibly time-varying but known orthonormal vectors  $y_a(t)$  and  $z_a(t)$ . Since we do not know  $\Omega_a^u$ , we can reconsider the feed-forward term in (27) with the control law

$$\Omega(R_e) = -k_w \log(R_e) + \text{Ad}_{R_e^\top}(\Omega_a^k). \quad (30)$$

Although we cannot compensate the unknown velocity in (29), let us consider it bounded, i.e.,  $\|\Omega_a^u(t)\| \leq \omega_d$ . In such a case, the control law (30) will not align  $R$  and  $R_a$  perfectly; nevertheless, since the geodesic distance (28) is exponentially stable with (27) in (4), then a bounded *disturbance* will shift the equilibrium point close to the origin, i.e.,  $\mu_r = 0$ . In fact, the bigger the control gain  $k_w$  the closer the shifted equilibrium point is to the origin. In particular, the dynamics (4) and the control law (30) considering (29) with the unknown but bounded angular velocity make the attitude  $R$  to converge exponentially fast, if  $\text{tr}(R_e(t_0)) \neq -1$  [30], to the following set:

**Definition 3** (Target attitude set). Consider  $x(t) \in S^2, R_a(t) \in \text{SO}(3)$  with  $R_a(t) = [m_d(t) \ * \ *]$  and a positive constant  $\delta \in [0, \pi]$ , the target attitude set is defined as

$$\mathcal{M}_\delta := \{R \mid \arccos(x(t)^\top m_d(t)) \leq \delta\}.$$

Furthermore, if  $k_w = \sqrt{2} \frac{\omega_d}{\mu_{R_e}^*}$ , then  $R(t) \rightarrow \mathcal{M}_{\delta^*}$ , where  $\mu_{R_e}^* \leq \delta^*$  [30].

### C. Study of the transitory alignment of 3D unicycles with the guiding vector field of ascending directions

In this subsection we are going to show how all the unicycles in the swarm can align with  $R_a(t)$  with an arbitrary precision in a compact set where  $\|\nabla \sigma(p)\| \geq \epsilon$ .

We first need to asses how far away the unicycles can get from each other, in order to guarantee that for generic initial attitudes  $R_i(0)$  and positions  $p_i(0)$ , the robots will not fall in a degenerated deployment  $x$ . For the sake of conciseness, let us consider that the unicycles have been already attracted to the invariant set  $\mathcal{M}_\delta^*$  with  $\delta^*$  sufficiently small. Indeed, for initial conditions out of  $\mathcal{M}_\delta^*$ , we would need to account for the individual travelled distances until the robots reach, exponentially fast,  $\mathcal{M}_\delta^*$  in order to apply the following result. Nevertheless, we can assume that  $p_{ij}(t^*) := p_i(t^*) - p_j(t^*)$ , being  $t^*$  the time once all robots' attitude are in  $\mathcal{M}_\delta^*$ , is equivalent to a non-degenerated deployment  $x$ .

**Proposition 7.** [30] *Given two robots  $i, j$  with dynamics (4),  $\|v\| = 1$  and a desired attitude matrix  $R_a(t) \in \text{SO}(3)$  with a target angular velocity (29) whose unknown contribution is bounded by  $\omega_d$ . If  $\Omega_{\{i,j\}}$  is given by the control law (30) with  $k_w = \sqrt{2} \frac{\omega_d}{\mu_{R_e}^*}$ ,  $R_{i,j}(t^*) \in \mathcal{M}_{\delta^*}$  with  $\delta^*$  sufficiently small and  $\mu_{R_e}^{\{i,j\}} = \mu_{R_e}^* \leq \delta^*$ , then*

$$\|p_{ij}(t) - p_{ij}(t^*)\| \leq \frac{2\sqrt{3}\mu_{R_e}^*}{k_w}.$$

Proposition 7 can be explained by noting that both robots  $i$  and  $j$  converge exponentially fast to the same attitude, but

different from  $R_a(t)$ , with the same rate of convergence. The analysis in [30] requires a small  $\delta^*$  to discard high order terms, similarly as in [38, Theorem 4.7], to assess the exponential stability of the equilibrium for the relative 3D attitudes in order to being able to calculate the integral of a relative velocity that is vanishing exponentially; thus, bounding the relative position  $p_{ij}(t), \forall t > t^*$ . We highlight that for 2D unicycles, i.e., the attitude is described by only one angle, the exponential stability of the relative headings is almost global, i.e., we discard the initial relative heading  $\pm\pi$ .

Since the alignment of all the unicycles' attitudes with  $R_a(t)$  occurs exponentially fast while guaranteeing that  $p_{ij}(t)$  remains bounded for all  $t$ , i.e., ensuring that  $x(t)$  is not degenerated, we can always find a common gain  $k_\omega^*$  for (30) such that if  $p_c(0) \in \mathcal{S}$ —the annulus shell centered at the signal's maximum  $p_\sigma$ —then all  $R_i(t)$  will align with  $R_a(t)$  with arbitrary precision before  $p_c$  leaves  $\mathcal{S}$ . Indeed, since  $\|\dot{p}_c(t)\| \leq 1$  and both the gradient and Hessian are bounded in  $\mathcal{S}$ , it follows that  $\|\dot{m}_d(t)\|$  and  $\|\Omega_a\|$  are also bounded within  $\mathcal{S}$ . We refer interested readers to [39] for the detailed calculations of these bounds.

#### D. Solution to the source-seeking problem with 3D unicycles

From Proposition 7, we know that given an initial non-degenerate  $x$  and a sufficiently high  $k_\omega$ , the computed  $L_\sigma$  within the annulus shell  $\mathcal{S}$  is an ascending direction given  $x(t)$  satisfies Proposition 1, i.e., the robot swarm will exit  $\mathcal{S}$  towards the signal source  $p_\sigma$ . Let us formalize this with the following main result.

**Theorem 2.** Consider a signal  $\sigma$  as in Definition 2 and a robot swarm of  $N$  unicycle robots with dynamics as in (4) with initial attitudes  $R_i(0)$  and initial positions  $p_i(0)$  such that the initial deployment  $x(0)$  is not degenerated. Let  $\epsilon > 0$  for Problem 1, then there exists a  $\kappa_\omega^* > 0$  such that if  $\kappa_\omega > \kappa_\omega^*$  in (30) with  $R_a(t)$  as in Definition 3 with  $\|\Omega_a^u(t)\| \leq \omega_d$  is a solution to the source-seeking Problem 1 given the conditions of Proposition 1 for an annulus shell  $\mathcal{S}$  around  $p_\sigma$ .

*Proof.* Similarly as in Theorem 1, consider an annulus shell  $\mathcal{S}$  with radii  $\epsilon^+ > \epsilon_- > 0$ , then, according to the Definition 2, if  $p_c \in \mathcal{S}$ , we know that there exist a  $D^*$  such that  $L_\sigma(p_c)$  is an ascending direction for a non-degenerated deployment  $x$  with  $\|x_i\| < D^*, \forall i$ . As it has been shown in Theorem 1, we know that tracking the ascending direction  $\frac{L_\sigma(p_c)}{\|L_\sigma(p_c)\|}$  with the  $X$  body-axes of the robots will guide the centroid of the swarm to at least a distance  $\epsilon_-$  from the source  $p_\sigma$ . We know from Proposition 7 that based on  $\mathcal{S}$  and the speed of the unicycles, we can calculate the required gain  $\kappa_\omega^*$  such that all the robots in the swarm will be aligned with  $R_a(t)$  within  $M_\delta^*$  and the deployment  $x$  will not be degenerated since the relative positions between the robots are bounded, e.g., the higher the gain  $\kappa_\omega^*$  the less the deformation of  $x(t)$  from  $x(0)$ . Indeed, there is a minimum  $\delta^*$  such that all  $X$  body-axes from the attitudes  $R_i(t)$  point at an ascending direction, i.e., a small deviation from  $L_\sigma(p_c)$  is still an ascending direction in  $\mathcal{S}$  if we choose a more conservative  $D^*$ . Note that the deviation of the actual tracked direction from  $L_\sigma$  depends

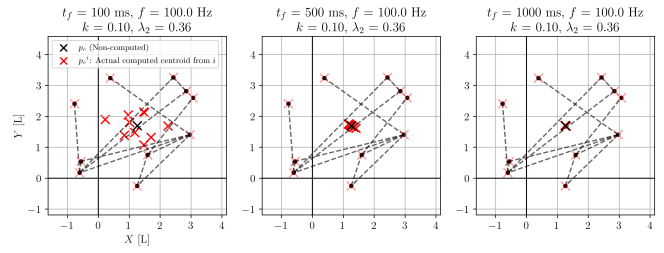


Fig. 10. Three snapshots from the algorithm that estimates the centroid of a robot swarm distributively. We can note the asymptotic convergence to the actual value of the centroid ( $X$  in black color), the  $X$  is red color is the current value. Each robot starts with  $x_i(0) = 0$  which is equivalent to start from their own positions, which is in light red color. The algorithm runs at 100 times per time unit, e.g., seconds. The dashed lines represent neighboring robots.

continuously on the bound  $\omega_d$ , with no deviation for  $\omega_d = 0$ . Thus, there is a time  $T^*$  such that  $\|p_c(T^*) - p_\sigma\| < \epsilon_-$  so the centroid leaves  $\mathcal{S}$ .

After leaving  $\mathcal{S}$ , if the centroid of the swarm enters it again, and the external radius  $\epsilon^+$  of  $\mathcal{S}$  is large enough, it will take a finite time until all the robot attitudes enter in  $M_\delta^*$  again since it is exponentially attractive; hence, the centroid of the swarm will leave again  $\mathcal{S}$  at time  $T_2^*$  such that  $\|p_c(T_2^*) - p_\sigma\| < \epsilon_-$  with  $T_2^* > T^*$ . Consequently, the trajectory of the centroid  $p_c(t)$  is trapped at least in a, very conservative, ball with radius  $\epsilon^+$  around the source  $p_\sigma$  as required by Problem 1. Since  $\frac{L_\sigma}{\|L_\sigma\|}$  is not defined in a set of measurement zero and outside of  $\mathcal{S}$ , in case of  $L_\sigma = 0$ , the robot swarm can track the immediately before computed direction.  $\square$

*Remark 5.* If the estimation of the ascending direction is done via the two consensus algorithms described in Figure 9, then the bounds given in Theorems 1 and 2 will be even more conservative since the centroid and ascending directions calculated distributively by the robots are not exactly the eventual asymptotic values considered in the main results.  $\blacktriangleleft$

## VII. NUMERICAL SIMULATIONS

All the numerical validations and simulations can be found in the following repository [https://github.com/Swarm-Systems-Lab/source\\_seeking](https://github.com/Swarm-Systems-Lab/source_seeking).

#### A. Distributed estimation of the swarm centroid

We show a numerical validation of Proposition 6 in Figure 10. In particular, for the following set of edges  $\mathcal{E} = \{(0, 2), (0, 5), (0, 3), (3, 9), (9, 8), (8, 4), (8, 1), (1, 7), (3, 6), (8, 1), (9, 2), (5, 9)\}$  associated with an algebraic connectivity  $\lambda_2 = 0.26$ . All the robots estimate asymptotically the centroid of the swarm with respect to their own positions, i.e., the barycentric coordinates  $-x_i$ .

#### B. Distributed source-seeking with single integrators

In Figure 11, we deploy 250 single-integrator robots within an area with the non-convex signal

$$\sigma(p) = 2 - 0.04 \|(p - p_\sigma)\| + \exp\{-0.9(p - p_\sigma)^T A_1 u_X\} + \exp\{0.9(p - p_\sigma)^T S^T A_2 S u_Y\},$$

where  $u_X = \begin{bmatrix} 1 \\ 0 \end{bmatrix}$ ,  $u_Y = \begin{bmatrix} 0 \\ 1 \end{bmatrix}$ ,  $p_\sigma = 40(u_X + u_Y)$ ,  $A_1 = \begin{bmatrix} \frac{1}{\sqrt{30}} & 0 \\ 1 & 0 \end{bmatrix}$ ,  $A_2 = \begin{bmatrix} 1 & 0 \\ 1 & \frac{1}{\sqrt{15}} \end{bmatrix}$  and  $S = \begin{bmatrix} 1 & -1 \\ 1 & 1 \end{bmatrix}$ , and they track the estimated direction of  $L_\sigma$  in Theorem 1, i.e., robots move at an unitary speed. Both, the centroid and the ascending direction are calculated distributively. The swarm starts as a uniform rectangular distribution. We show the resilience of the swarm by introducing the following three factors. Firstly, in order to show *misplacements* within the formation, we inject noise to the actuators, i.e., every 0.2 time units the robots track the direction  $L_\sigma$  with a random deviation within  $\pm 10$  degrees. Secondly, the swarm maneuvers between two white circles by morphing its shape. Thirdly, there is a random probability for individual robots to stop functioning, i.e., they stop moving and do not belong to the network anymore. In fact, at time 6.5 the network splits into two *disconnected* swarms. These *dead* robots are represented in red color, and only 80 robots made it eventually to the source. Eventually, the centroid swarm gets so close to the source that  $L_\sigma$  becomes unreliable, i.e., the centroid entered the  $\epsilon$ -ball in Problem 1.

### C. Distributed source-seeking with unicycles

In Figures 12 and 13 we show the effectiveness of Theorem 2 with unicycles travelling at constant speeds in both 2D and 3D respectively. In both cases the agents start with arbitrary directions but they converge to the same one close to the given by  $L_\sigma$ . We note that once the swarm centroid gets close enough to the source, the agents start describing close orbits. In this way, the distance between the centroid and the source gets bounded.

## VIII. CONCLUSION

We have presented a distributed, robust, and resilient source-seeking algorithm for robot swarms. The robots are capable of determining an ascending direction and aligning with it to locate the source of a scalar field. We have provided sufficient conditions for the algorithm's effectiveness and analyzed the sensitivity of the ascending direction. Specifically, the ascending direction is nearly parallel to the gradient in cases where the shape exhibits certain symmetries and when the spatial deployment variance is equal across all orthogonal directions. In order to have a self-contained article, we have also presented a distributed algorithm for the calculation of the barycentric coordinates of the robots. Finally, we have demonstrated the effectiveness of our strategy for both 2D and 3D robots moving at constant speeds, with their centroid coming arbitrarily close to the source of the scalar field.

## REFERENCES

- [1] P. Ogren, E. Fiorelli, and N. E. Leonard, "Cooperative control of mobile sensor networks: Adaptive gradient climbing in a distributed environment," *IEEE Transactions on Automatic Control*, vol. 49, no. 8, pp. 1292–1302, 2004.
- [2] V. Kumar, D. Rus, and S. Singh, "Robot and sensor networks for first responders," *IEEE Pervasive computing*, vol. 3, no. 4, pp. 24–33, 2004.
- [3] K. McGuire, C. De Wagter, K. Tuyls, H. Kappen, and G. C. de Croon, "Minimal navigation solution for a swarm of tiny flying robots to explore an unknown environment," *Science Robotics*, vol. 4, no. 35, p. eaaw9710, 2019.
- [4] W. Li, J. A. Farrell, S. Pang, and R. M. Arrieta, "Moth-inspired chemical plume tracing on an autonomous underwater vehicle," *IEEE Transactions on Robotics*, vol. 22, no. 2, pp. 292–307, 2006.
- [5] J. N. Twigg, J. R. Fink, L. Y. Paul, and B. M. Sadler, "Rss gradient-assisted frontier exploration and radio source localization," in *2012 IEEE International Conference on Robotics and Automation*. IEEE, 2012, pp. 889–895.
- [6] G.-Z. Yang, J. Bellingham, P. E. Dupont, P. Fischer, L. Floridi, R. Full, N. Jacobstein, V. Kumar, M. McNutt, R. Merrifield *et al.*, "The grand challenges of science robotics," *Science robotics*, vol. 3, no. 14, p. eaar7650, 2018.
- [7] M. Brambilla, E. Ferrante, M. Birattari, and M. Dorigo, "Swarm robotics: a review from the swarm engineering perspective," *Swarm Intelligence*, vol. 7, pp. 1–41, 2013.
- [8] M. Dorigo, G. Theraulaz, and V. Trianni, "Swarm robotics: Past, present, and future [point of view]," *Proceedings of the IEEE*, vol. 109, no. 7, pp. 1152–1165, 2021.
- [9] W. Yao, H. G. de Marina, B. Lin, and M. Cao, "Singularity-free guiding vector field for robot navigation," *IEEE Transactions on Robotics*, vol. 37, no. 4, pp. 1206–1221, 2021.
- [10] W. Yao, H. G. de Marina, Z. Sun, and M. Cao, "Guiding vector fields for the distributed motion coordination of mobile robots," *IEEE Transactions on Robotics*, 2022.
- [11] F. Bullo and R. M. Murray, "Tracking for fully actuated mechanical systems: a geometric framework," *Automatica*, vol. 35, no. 1, pp. 17–34, 1999.
- [12] E. Rosero and H. Werner, "Cooperative source seeking via gradient estimation and formation control," in *2014 UKACC International Conference on Control (CONTROL)*. IEEE, 2014, pp. 634–639.
- [13] S. A. Barogh and H. Werner, "Cooperative source seeking with distance-based formation control and non-holonomic agents," *IFAC-PapersOnLine*, vol. 50, no. 1, pp. 7917–7922, 2017.
- [14] L. Briñón-Arranz, L. Schenato, and A. Seuret, "Distributed source seeking via a circular formation of agents under communication constraints," *IEEE Transactions on Control of Network Systems*, vol. 3, no. 2, pp. 104–115, 2015.
- [15] L. Briñón-Arranz, A. Renzaglia, and L. Schenato, "Multirobot symmetric formations for gradient and hessian estimation with application to source seeking," *IEEE Transactions on Robotics*, vol. 35, no. 3, pp. 782–789, 2019.
- [16] R. Fabbiano, F. Garin, and C. Canudas-de Wit, "Distributed source seeking without global position information," *IEEE Transactions on Control of Network Systems*, vol. 5, no. 1, pp. 228–238, 2016.
- [17] Z. Li, K. You, and S. Song, "Cooperative source seeking via networked multi-vehicle systems," *Automatica*, vol. 115, p. 108853, 2020.
- [18] J. Cochran and M. Krstic, "Nonholonomic source seeking with tuning of angular velocity," *IEEE Transactions on Automatic Control*, vol. 54, no. 4, pp. 717–731, 2009.
- [19] E. Bryk and M. Arcaç, "Gradient climbing in formation via extremum seeking and passivity-based coordination rules," *Asian Journal of Control*, vol. 10, no. 2, pp. 201–211, 2008.
- [20] S. Al-Abri and F. Zhang, "A distributed active perception strategy for source seeking and level curve tracking," *IEEE Transactions on Automatic Control*, vol. 67, no. 5, pp. 2459–2465, 2021.
- [21] T. Zhang, V. Qin, Y. Tang, and N. Li, "Distributed information-based source seeking," *IEEE Transactions on Robotics*, 2023.
- [22] B. Bayat, N. Crasta, H. Li, and A. Ijspeert, "Optimal search strategies for pollutant source localization," in *2016 IEEE/RSJ International Conference on Intelligent Robots and Systems (IROS)*. IEEE, 2016, pp. 1801–1807.
- [23] M. S. Lee, D. Shy, W. R. Whittaker, and N. Michael, "Active range and bearing-based radiation source localization," in *2018 IEEE/RSJ International Conference on Intelligent Robots and Systems (IROS)*. IEEE, 2018, pp. 1389–1394.
- [24] J. Cortes, S. Martinez, T. Karatas, and F. Bullo, "Coverage control for mobile sensing networks," *IEEE Transactions on Robotics and Automation*, vol. 20, no. 2, pp. 243–255, 2004.
- [25] A. Benevento, M. Santos, G. Notarstefano, K. Paynabar, M. Bloch, and M. Egerstedt, "Multi-robot coordination for estimation and coverage of unknown spatial fields," in *2020 IEEE International Conference on Robotics and Automation (ICRA)*. IEEE, 2020, pp. 7740–7746.
- [26] A. Acuaviva, J. Bautista, W. Yao, J. Jimenez, and H. G. de Marina, "Resilient source seeking with robot swarms," in *2024 Conference on Decision and Control*, 2024.

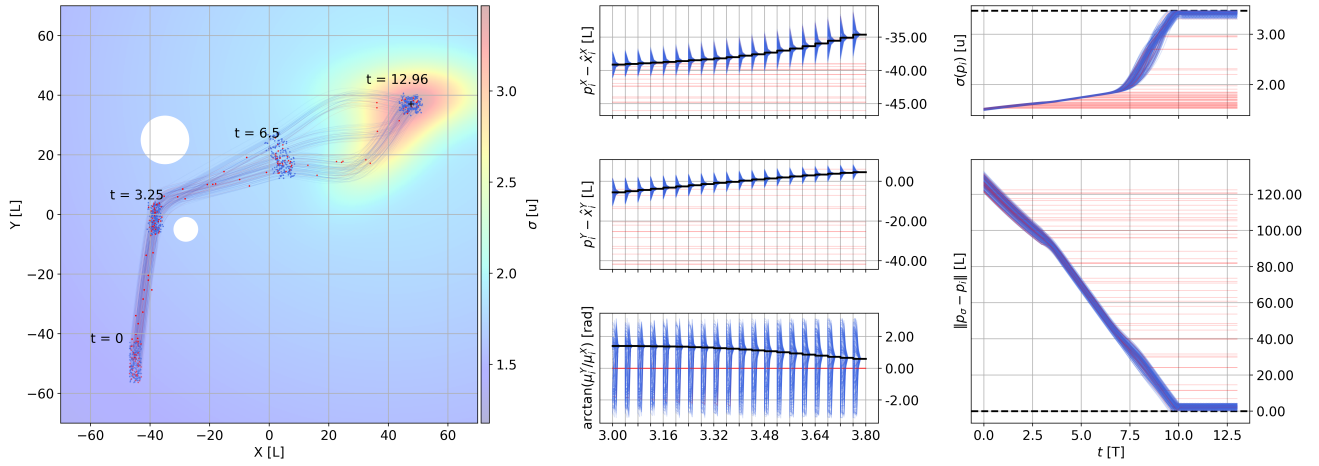


Fig. 11. A robot swarm of 250 single-integrators (blue dots) faces faulty actuators with noisy directions, and also individuals stop working randomly (turned into red dots). The swarm can maneuver by morphing its shape, e.g., to pass between the two white circles, and reaches the signal source eventually, where 170 robots were dead during the mission. Furthermore, due to the dead robots, the network splits into two at time 6.5; therefore, creating two independent swarms. Nonetheless, the *alive* robots made it to the source, demonstrating the resiliency of the swarm. At the middle, from top to down for a short time, in black color the position  $p_c^{\{X,Y\}}$  and in blue the corresponding estimations of the robots. In red color are the dead robots. At the bottom, in black color the actual ascending direction  $L_\sigma$  and in blue the estimated direction by the robots. At the right side, above, the signal reading by the robots in blue and in black dashed the value of the source. Below, the norm of the relative position between the robots and the source.

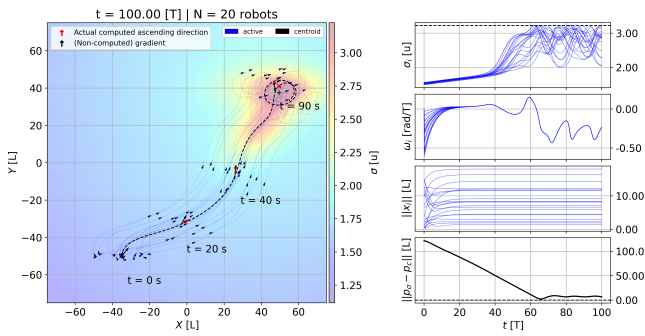


Fig. 12. A robot swarm of 20 2D unicycles travelling at constant speed orbits around the signal source. At the right side, from top to bottom, firstly, the signal reading of each robot in blue; secondly, the angular velocity of all the agents; thirdly, the distance of the robots regarding their centroid; lastly, the distance of the centroid to the signal source.

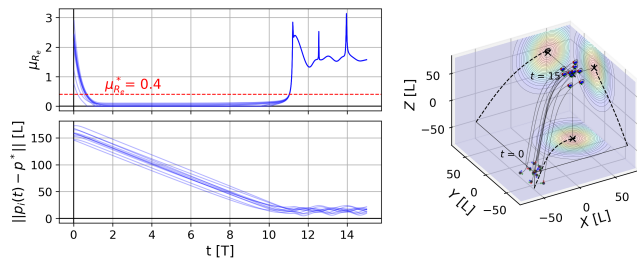


Fig. 13. A robot swarm of 50 3D unicycles travelling at a constant speed. At the left side, on top the alignment error of the agents with the guiding vector field; note that it grows once the agents are close to the source where the guiding vector field varies rapidly. Below, the distance of the centroid to the signal source decreases over time and remains bounded.

- [27] F. Bullo, *Lectures on network systems*. Kindle Direct Publishing, 2020, vol. 1.
- [28] F. Bullo and A. D. Lewis, *Geometric Control of Mechanical Systems*, ser. Texts in Applied Mathematics. New York-Heidelberg-Berlin: Springer Verlag, 2004, vol. 49.
- [29] J. Solà, J. Deray, and D. Atchuthan, “A micro lie theory for state estimation in robotics,” *arXiv*, 2021.
- [30] J. Bautista and H. G. de Marina, “So(3) attitude controllers and the alignment of robots with non-constant 3d vector fields,” *arXiv*, 2024.
- [31] A. Clauset, C. R. Shalizi, and M. E. Newman, “Power-law distributions in empirical data,” *SIAM review*, vol. 51, no. 4, pp. 661–703, 2009.
- [32] W. Rudin, *Principles of mathematical analysis*, 3rd ed. McGraw-hill New York, 1976.
- [33] K.-K. Oh, M.-C. Park, and H.-S. Ahn, “A survey of multi-agent formation control,” *Automatica*, vol. 53, pp. 424–440, 2015.
- [34] H. G. de Marina, “Maneuvering and robustness issues in undirected displacement-consensus-based formation control,” *IEEE Transactions on Automatic Control*, vol. 66, no. 7, pp. 3370–3377, 2020.
- [35] H. Zhang, F. L. Lewis, and A. Das, “Optimal design for synchronization of cooperative systems: state feedback, observer and output feedback,” *IEEE Transactions on Automatic Control*, vol. 56, no. 8, pp. 1948–1952, 2011.
- [36] R. Olfati-Saber and R. M. Murray, “Consensus problems in networks of agents with switching topology and time-delays,” *IEEE Transactions on automatic control*, vol. 49, no. 9, pp. 1520–1533, 2004.
- [37] Y. A. Kapityuk, A. V. Proskurnikov, and M. Cao, “A guiding vector-field algorithm for path-following control of nonholonomic mobile robots,” *IEEE Transactions on Control Systems Technology*, vol. 26, no. 4, pp. 1372–1385, 2017.
- [38] H. K. Khalil, *Nonlinear control*. Pearson New York, 2015.
- [39] A. Acuaviva, “Source-seeking problem with robot swarms,” *Bachelor’s thesis, arXiv preprint: <https://arxiv.org/abs/2408.10152>*, 2022.